International Journal of Nanomedicine

Dovepress
Taylor & Francis Group

Open Access Full Text Article

ORIGINAL RESEARCH

Harnessing *Levilactobacillus brevis* as a Microbial Nanofactory for the Sustainable Production of Multifunctional Silver Nanoparticles

Mervat G Hassan[1], Sameh S Ali[2], Hadeer Y Abdel-Aziz[1], Mohamed O Abdel-Monem[1], Mahmoud M Amer[1], Mona Abd El-Aziz Gadallah[3], Michael Schagerl[4], Amr A El-Waseif[5]

[1]Botany and Microbiology Department, Faculty of Science, Banha University, Banha, Egypt; [2]Botany and Microbiology Department, Faculty of Science, Tanta University, Tanta, 31527, Egypt; [3]Medical Microbiology and Immunology Department, Faculty of Medicine, Tanta University, Tanta, 31527, Egypt; [4]Department of Functional and Evolutionary Ecology, University of Vienna, Vienna, A-1030, Austria; [5]Botany and Microbiology Department, Faculty of Science (Boys), Al-Azhar University, Cairo, Egypt

Correspondence: Sameh S Ali; Michael Schagerl, Email samh_samir@science.tanta.edu.eg; michael.schagerl@univie.ac.at

Introduction: Green synthesis of silver nanoparticles (AgNPs) using probiotic microorganisms has emerged as a sustainable strategy for producing multifunctional nanomaterials with enhanced biomedical potential. In the present study, the probiotic bacterium *Levilactobacillus brevis*, isolated from raw milk and identified by 16S ribosomal ribonucleic acid (16S rRNA) gene sequencing under GenBank accession number PZ476340, was employed as a biological reducing and stabilizing agent for AgNP biosynthesis.

Methods: Nanoparticle formation was initially confirmed by a characteristic color change and subsequently characterized using ultraviolet–visible (UV–Vis) spectroscopy, Fourier transform infrared spectroscopy (FTIR), transmission electron microscopy (TEM), selected area electron diffraction (SAED), and zeta potential analysis. The biological activities of the biosynthesized AgNPs were evaluated through 2,2-diphenyl-1-picrylhydrazyl (DPPH) radical scavenging antioxidant assay, 3-(4,5-dimethylthiazol-2-yl)-2,5-diphenyltetrazolium bromide (MTT) cytotoxicity assay, in vitro scratch wound-healing assay, and anticoagulant assays based on prothrombin time (PT) and activated partial thromboplastin time (APTT).

Results: UV–Vis spectroscopy revealed a distinct surface plasmon resonance peak at approximately 410 nm, confirming the formation of AgNPs. FTIR analysis demonstrated the involvement of extracellular proteins and polysaccharides in nanoparticle reduction and surface capping, while TEM and SAED analyses showed predominantly spherical, crystalline nanoparticles with sizes ranging from 7 to 55 nm and an average diameter of 27.18 ± 12.7 nm. Zeta potential analysis yielded a value of −2.57 mV, indicating weak electrostatic stabilization; however, FTIR data suggested that colloidal stability was primarily maintained through steric hindrance provided by a biomolecular capping layer derived from *L. brevis* metabolites. The nanoparticles exhibited strong concentration-dependent antioxidant activity, achieving 79.7% DPPH radical scavenging at 1000 µg/mL, with a half-maximal inhibitory concentration (IC_{50}) of 61.4 µg/mL. MTT assays demonstrated significant dose-dependent cytotoxicity against Vero normal kidney epithelial, MCF-7 human breast adenocarcinoma, and HepG2 human hepatocellular carcinoma cell lines, with IC_{50} values of 110.29, 81.28, and 102.64 µg/mL, respectively, accompanied by marked morphological alterations. In vitro scratch assays revealed moderate wound-healing activity, resulting in approximately 34.5% wound closure after 48 h. Furthermore, the AgNPs exhibited anticoagulant activity by prolonging PT and APTT, suggesting interactions with coagulation pathways.

Conclusion: Collectively, these findings demonstrate that *L. brevis* can serve as an efficient microbial nanofactory for the eco-friendly synthesis of multifunctional AgNPs. The combination of nanoscale dimensions, crystalline structure, and biomolecular surface functionalization contributed to significant antioxidant, cytotoxic, wound-healing, and anticoagulant activities, highlighting the potential of probiotic-mediated nanotechnology for biomedical and therapeutic applications.

Keywords: silver nanoparticles, probiotic-mediated nanotechnology, biomedical nanomaterials

https://doi.org/10.2147/IJN.S612998
Received: 31 March 2026
Accepted: 30 June 2026
Published: 21 July 2026

Introduction

Nanotechnology has revolutionized material science and biomedicine by enabling the design and fabrication of nanomaterials with unique physicochemical properties distinct from their bulk counterparts. These properties include a high surface-area-to-volume ratio, tunable optical characteristics, enhanced catalytic activity, and distinctive electrical and thermal behaviors, which allow nanoparticles to interact with biological systems in precise and targeted ways.[1,2] Such capabilities have significantly expanded the biomedical applications of nanoparticles, encompassing drug delivery, diagnostics, antimicrobial therapies, tissue engineering, and therapeutic interventions. Metallic nanoparticles, particularly silver nanoparticles (AgNPs), have attracted considerable attention due to their structural stability, versatile functional properties, and broad-spectrum biological activity.[3]

Silver nanoparticles are renowned for their potent antimicrobial, anti-inflammatory, antioxidant, and wound-healing activities, making them invaluable in clinical and pharmaceutical contexts.[4–7] Their effectiveness against diverse pathogenic microorganisms, including antibiotic-resistant strains, has facilitated their incorporation into wound dressings, medical device coatings, dental materials, textiles, and other therapeutic formulations.[5,6] Beyond antimicrobial effects, AgNPs have demonstrated significant antioxidant and anticancer potential, enabling applications that extend to oxidative stress mitigation and cancer therapy. These multifunctional properties render AgNPs attractive candidates for next-generation biomedical nanomaterials capable of addressing multiple clinical challenges simultaneously.

Conventionally, AgNPs are synthesized using physical and chemical methods, which often require high energy input, specialized instrumentation, and toxic reducing agents, thereby raising concerns regarding environmental impact, cytotoxicity, and clinical biocompatibility.[8,9] Moreover, nanoparticles synthesized through these approaches may suffer from aggregation, poor stability, and suboptimal biological activity. To overcome these limitations, green synthesis strategies employing biological systems have emerged as sustainable, cost-effective, and scalable alternatives. Biological synthesis utilizes naturally occurring biomolecules from plants, fungi, algae, and microorganisms to reduce metal ions and stabilize nanoparticles, producing nanostructures coated with bioactive molecules that enhance their functional performance and biocompatibility.[10–12]

Microorganisms, in particular, serve as efficient nano-biofactories due to their rapid growth, metabolic versatility, and ability to secrete extracellular biomolecules that facilitate nanoparticle formation and stabilization. Probiotic bacteria have garnered increasing interest as microbial nanofactories because of their generally recognized as safe (GRAS), and capacity to produce bioactive metabolites, including enzymes, proteins, and polysaccharides, which can act as reducing and capping agents.[13–17] Biologically synthesized AgNPs from microbial sources have been shown to exhibit enhanced biomedical activities, including antimicrobial, antioxidant, wound-healing, and cytotoxic effects. Nevertheless, most studies focus on individual functional attributes rather than the simultaneous assessment of multifunctional biomedical properties.

Chronic wounds are a significant global health burden, often associated with impaired hemostasis and prolonged inflammation, which complicate tissue repair and increase susceptibility to infection.[18] Silver nanoparticles have been reported not only to promote wound healing through antimicrobial and antioxidant mechanisms but also to interact with blood clotting factors, thereby modulating coagulation pathways. Specifically, AgNPs can influence the intrinsic and extrinsic coagulation cascades by interacting with fibrinogen, thrombin, and platelet aggregation processes, potentially altering prothrombin time and activated partial thromboplastin time.[19] These interactions provide a mechanistic basis for evaluating the anticoagulant potential of biosynthesized AgNPs, which is particularly relevant in designing multifunctional nanomaterials capable of both promoting tissue repair and preventing pathological clot formation.

Despite the promise of probiotics for nanoparticle synthesis, specific probiotic strains such as *Levilactobacillus brevis* remain underexplored in the context of multifunctional AgNP production. While several Lactobacillus and Bifidobacterium species have been investigated for nanoparticle biosynthesis, the ability of *L. brevis* to act as a microbial nanofactory producing silver nanoparticles with combined antioxidant, cytotoxic/anticancer, wound-healing, and anticoagulant activities has not been systematically studied. This represents a significant knowledge gap, as probiotic-mediated biosynthesis may offer enhanced biocompatibility, reduced cytotoxicity to normal cells, and potential

synergistic therapeutic effects. Furthermore, leveraging *L. brevis* aligns with sustainable and eco-friendly nanotechnology approaches, reducing reliance on chemical reagents and energy-intensive processes.

Accordingly, the present study focuses on the biosynthesis of silver nanoparticles using the probiotic bacterium *L. brevis* as a biological reducing and stabilizing agent. The synthesized nanoparticles were comprehensively characterized using spectroscopic and microscopic techniques to determine their structural, morphological, and colloidal properties. In parallel, their multifunctional biomedical potential was evaluated through in vitro antioxidant, cytotoxic/anticancer, wound-healing, and anticoagulant assays. By combining the use of a probiotic nano-biofactory with thorough functional evaluation, this study provides critical insights into the potential of *L. brevis*-derived silver nanoparticles as sustainable and multifunctional nanomaterials for biomedical applications. Overall, this work not only advances the field of probiotic-mediated nanoparticle synthesis but also highlights the significance of developing environmentally friendly, multifunctional nanomaterials with enhanced biocompatibility and therapeutic potential. The findings offer a promising foundation for future applications of probiotic-synthesized AgNPs in clinical, pharmaceutical, and biomedical contexts.

Materials and Methods

Isolation, Purification, and Preliminary Characterization of Probiotic Lactic Acid Bacteria

Raw milk samples (n = 7) were collected aseptically from different rural locations in Egypt and transported to the laboratory under refrigerated conditions (4 C) for immediate processing. For each sample, 5 g of milk were homogenized in 20 mL sterile physiological saline (pH 7.0) for 2 min to ensure uniform dispersion of the microbial load. Aliquots of the homogenate were inoculated into de Man, Rogosa and Sharpe (MRS) broth (Oxoid Ltd., UK) and incubated at 37°C for 24 h. (pH 6.2), a selective medium optimized for lactic acid bacteria (LAB), and incubated aerobically at 37 °C for 24 h to enrich LAB populations.[20] Following enrichment, serial dilutions were prepared in sterile saline, and 20 µL of the appropriate dilutions were spread onto MRS agar plates. Plates were incubated at 37 °C for 48 h to allow development of discrete colonies.[21] Colonies exhibiting typical LAB morphology (small to medium, creamy-white/whitish, smooth colonies) were selected and purified by repeated streaking on fresh MRS agar (Oxoid Ltd., Basingstoke, Hampshire, UK) until single-colony purity was obtained. Each purified isolate was propagated in MRS broth (37 °C, 24 h) to obtain fresh cultures for screening and identification.

Preliminary characterization of the isolates was performed using standard phenotypic tests. Gram staining was carried out to confirm Gram-positive reaction and cell morphology (rod-shaped bacilli consistent with *Lactobacillus* spp.), and the catalase test was conducted using 3% (v/v) H_2O_2 to exclude catalase-positive contaminants. Only Gram-positive, catalase-negative isolates were retained for further study because these traits are consistent with LAB and widely used as initial selection criteria for probiotic candidates.[15] Pure isolates were preserved for downstream experiments by preparing glycerol stocks (final glycerol concentration 25%, w/v) and storing them at −80 °C to maintain genetic and phenotypic stability prior to nanoparticle biosynthesis and molecular identification. The overall experimental design employed in this study is illustrated in Figure 1.

Molecular Identification of the Selected Probiotic Isolate

Genomic deoxyribonucleic acid (DNA) of the selected isolate was extracted using the Wizard® Genomic DNA Purification Kit (Promega, Madison, WI, USA). The 16S rRNA gene was amplified using the universal primers Strep F (5′-AAGAGTTTGATCCTGGCTCAG-3′) and Strep R (5′-CTACGGCTACCTTGTTACGA-3′). Polymerase chain reaction (PCR) amplification was performed with an initial denaturation at 96 °C for 5 min, followed by 35 cycles of 96 °C for 1 min, 50 °C for 1 min, and 72 °C for 2 min, with a final extension at 72 °C for 2 min. PCR products were verified by 1% agarose gel electrophoresis, purified, and sequenced using the BigDye® Terminator v3.0 Cycle Sequencing Kit (Applied Biosystems, Foster City, CA, USA). Forward and reverse sequences were assembled into a consensus sequence and compared with sequences in the national center for biotechnology information (NCBI) GenBank database using basic local alignment search tool (BLAST). The obtained sequence was deposited in GenBank under accession number PZ476340. Phylogenetic analysis was conducted using the Maximum Likelihood method in MEGA12 with the Tamura–Nei model.[22–24]

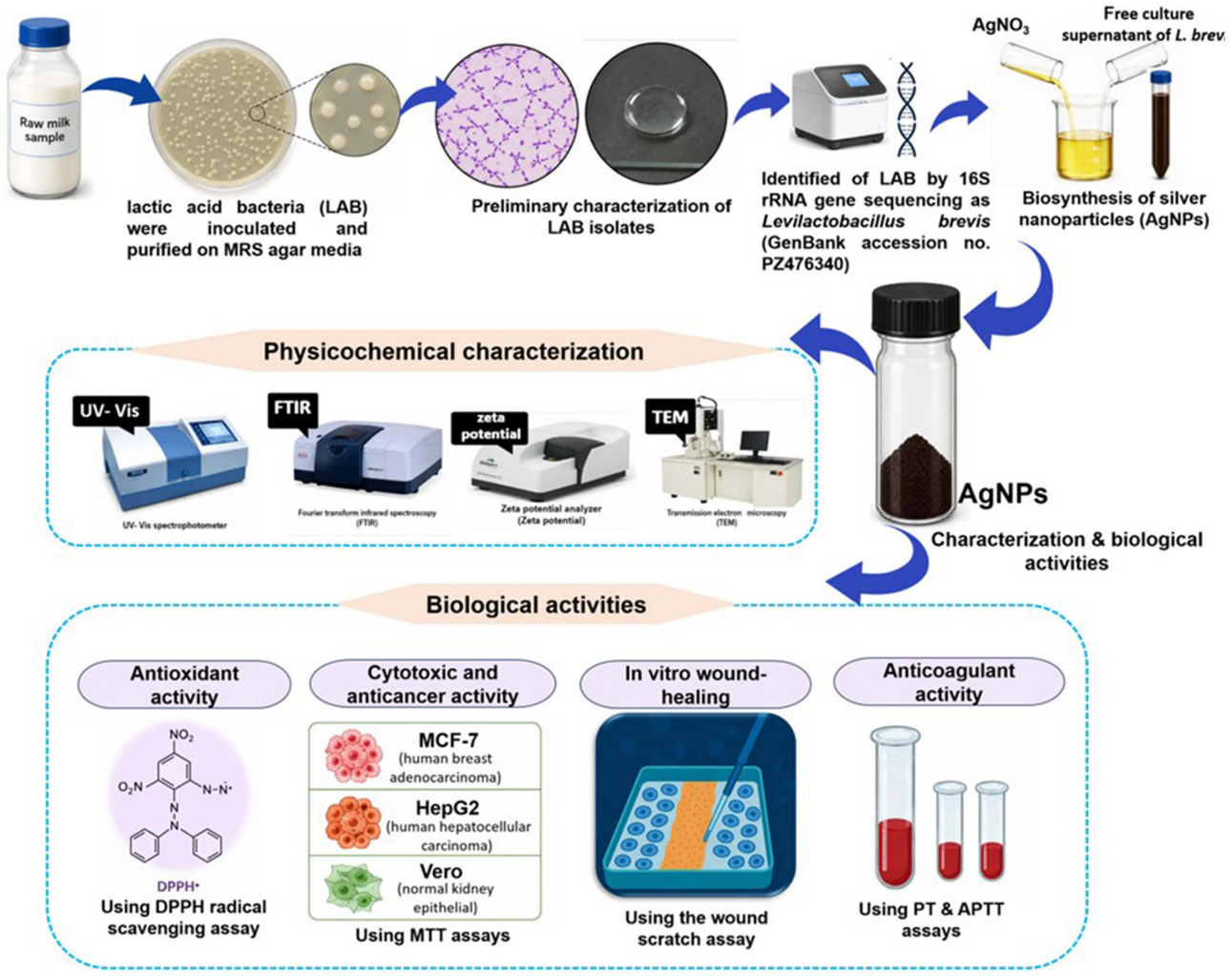

Figure 1 Experimental setup illustrating the biosynthesis of silver nanoparticles (AgNPs) using the cell-free culture supernatant, physicochemical characterization, and evaluation of antioxidant, cytotoxic/anticancer, wound-healing, and anticoagulant activities.

Cultivation of L. brevis for Nanoparticle Biosynthesis

The molecularly identified strain *L. brevis* was routinely maintained on MRS agar slants at 4 °C and periodically subcultured to ensure viability. For experimental scale-up, a loopful of the preserved culture was inoculated into sterile MRS broth (pH 6.2) and incubated at 30 °C for 24 h under static conditions. To ensure reproducibility and standardization of the inoculum across experimental replicates, bacterial growth was monitored until the late exponential phase was reached (OD_{600} = 0.6). At this stage, the biomass concentration was approximately 1.4 g/L prior to harvesting, providing a consistent source of extracellular metabolites involved in nanoparticle biosynthesis. The bacterial culture was subsequently centrifuged at 5000 rpm for 10 min to separate the biomass from the culture medium. The resulting cell-free supernatant was carefully collected and used as the biological reducing and stabilizing agent for the extracellular biosynthesis of silver nanoparticles. This approach eliminates the need for cell disruption, facilitates nanoparticle recovery, reduces downstream purification requirements, and enhances the scalability and reproducibility of the biosynthetic process.[6]

Biosynthesis of Silver Nanoparticles

AgNPs were biosynthesized using the cell-free culture supernatant of *L. brevis* as a biological reducing and stabilizing agent, following a previously described method with minor modifications.[25] Briefly, the bacterial culture was centrifuged at 5,000 rpm for 10 min to obtain a clear cell-free supernatant. A 1 mM aqueous silver nitrate ($AgNO_3$) solution was prepared by dissolving 0.017 g $AgNO_3$ in 100 mL sterile distilled water. Equal volumes of the cell-free supernatant and

$AgNO_3$ solution were mixed under aseptic conditions, and the pH of the reaction mixture was adjusted to 6.0. The reaction mixture was incubated overnight in the dark at 25 ± 2 °C to prevent photoreduction of silver ions. Nanoparticle formation was initially monitored by the characteristic color change of the reaction mixture from pale yellow to dark brown, indicating the reduction of Ag^+ ions to metallic silver nanoparticles by extracellular biomolecules present in the culture supernatant. The synthesized AgNPs were purified by repeated centrifugation and washing with sterile distilled water to remove residual silver ions and unbound biomolecules. The purified nanoparticles were then collected, and their yield was determined gravimetrically prior to physicochemical characterization and biological activity assessment.

Physicochemical Characterization of Biosynthesized Silver Nanoparticles

Comprehensive physicochemical characterization of the biosynthesized AgNPs was performed to evaluate their optical properties, morphology, particle size distribution, surface chemistry, and colloidal stability. To ensure data reliability, all instrument systems were calibrated prior to sample execution, and all measurements were conducted in triplicate (n = 3) with the resulting data averaged and processed as described below. The formation and optical properties of the AgNPs were monitored using a T80+ ultraviolet -visible spectroscopy (PG Instruments Ltd., UK). The instrument was calibrated using a holmium oxide filter for wavelength accuracy, and a photometric baseline correction was performed from 190 to 1000 nm against a distilled water blank. Absorbance spectra of the nanoparticle suspension were recorded at room temperature over the wavelength range of 190–1000 nm using a fast scan rate mode and a spectral resolution window of 1.0 nm. The characteristic surface plasmon resonance (SPR) absorption peak was utilized as a primary indicator of nanoparticle formation and dispersion quality.[26] To identify the organic functional groups responsible for the reduction, capping, and stabilization of the AgNPs, Fourier transform infrared spectroscopy (FTIR) was conducted.[27] The Nexus 670 FTIR spectrophotometer (Thermo Nicolet, USA) was calibrated against an internal polystyrene standard film to verify wavenumber accuracy. Dried nanoparticle samples were uniformly blended with spectroscopic-grade potassium bromide (KBr) at a weight ratio of 1:100 and compressed under 10 tons of hydraulic pressure into thin, translucent pellets. Spectra were recorded over the wavenumber range of 4000–400 cm^{-1} at a high spectral resolution of 4 cm^{-1}, accumulating 32 co-added scans per sample to optimize the signal-to-noise ratio. The raw interferograms were processed via a standard linear baseline correction approach to eliminate background slope variance prior to peak identification. The morphology, size distribution, and structural characteristics of the nanoparticles were evaluated via transmission electron microscopy (TEM; JEOL JXA-840A, Japan).[28] The TEM grid stage and magnification scale were calibrated using a certified gold nanoparticle grid standard. For analysis, a 10 μL drop of the diluted nanoparticle suspension was deposited onto a 200-mesh carbon-coated copper grid, allowed to dry completely under vacuum at room temperature, and imaged at an accelerating voltage of 80 kV. Micrographs were obtained across multiple grid fields to determine particle size histograms, geometry, and spatial dispersion patterns. The surface charge and colloidal stability of the AgNPs were measured using a NICOMP laser zeta potential analyzer (Molecule Measuring Systems, USA), calibrated with a certified latex standard solution (−50 mV). To minimize ionic interference and background scattering, a 5.0 mL aliquot of the nanoparticle suspension was diluted tenfold in 50 mL double-distilled water, gently agitated for 3 min, and allowed to equilibrate for 2 min at 25 °C. The pH of the solution was monitored during measurement. Although a zeta potential magnitude of ±30 mV is generally considered the threshold for high electrostatic stability, the biosynthesized AgNPs exhibited a low value of −2.57 mV, indicating weak electrostatic repulsion. This suggests that long-term colloidal stability is primarily maintained through steric stabilization provided by the dense biomolecular capping layer, as supported by FTIR analysis. All reported values represent the average of three independent measurements.

Biological Activity Evaluation of Biosynthesized Silver Nanoparticles

The biological activities of the biosynthesized AgNPs were evaluated through a series of in vitro assays to assess their antioxidant, cytotoxic/anticancer, wound-healing, and anticoagulant properties. All experiments were performed in triplicate (n = 3) under sterile conditions. Control treatments, including $AgNO_3$ solution and *L. brevis* culture supernatant alone, were included in all assays to distinguish nanoparticle-specific effects from those of the precursor solution or biological matrix.

Antioxidant Activity

The antioxidant activity of AgNPs was evaluated using the 2,2-diphenyl-1-picrylhydrazyl (DPPH) radical scavenging assay according to Huang et al,[29] A 0.1 mM DPPH solution was prepared in ethanol. Briefly, 3 mL of AgNP suspensions at different concentrations (3.9, 7.8, 15.62, 31.25, 62.5, 125, 250, 500, and 1000 μg/mL) were mixed with 1 mL of DPPH solution. The mixtures were vortexed and incubated at room temperature in the dark for 30 min. Absorbance was then measured at 517 nm using a UV–Vis spectrophotometer (Milton Roy, USA). Ascorbic acid was used as a positive control. All measurements were performed in triplicate. The percentage of DPPH radical scavenging activity was calculated using the following equation: DPPH scavenging activity (%) = $[(A_0 - A_1)/A_0] \times 100$, where A_0 is the absorbance of the control and A_1 is the absorbance of the sample. The half maximal inhibitory concentration (IC_{50}) value was determined from the concentration–response curve.[30]

Cytotoxicity and Anticancer Activity

The cytotoxic and anticancer activities of the biosynthesized AgNPs were assessed using the 3-(4,5-dimethylthiazol-2-yl)-2,5-diphenyltetrazolium bromide (MTT) assay against MCF-7 human breast adenocarcinoma, HepG2 human hepatocellular carcinoma, and Vero normal kidney epithelial cell lines. All cell lines were obtained from the American Type Culture Collection (ATCC, Rockville, MD, USA). The Vero cell line was derived from kidney epithelial cells of *Cercopithecus aethiops* and obtained as ATCC CCL-81, the MCF-7 cell line was derived from mammary gland, breast; derived from metastatic site: pleural effusion epithelial cells of Homo sapiens, human and obtained as ATCC HTB-22, and the HepG2 cell line was derived from liver epithelial cells of Homo sapiens, human and obtained as ATCC HB-8065.

Cells were seeded into 96-well tissue culture plates at a density of 1×10^5 cells/mL (100 μL per well) and incubated at 37 °C with 5% CO_2 for 24 h to allow formation of a confluent monolayer. After incubation, the monolayer was washed twice with phosphate-buffered saline (PBS) to remove non-adherent cells, and fresh Roswell Park Memorial Institute (RPMI) medium containing serial dilutions of AgNPs was added. Control wells received culture medium only. The plates were incubated at 37 °C with 5% CO_2, and cells were examined microscopically for morphological changes indicative of cytotoxicity, such as shrinkage, rounding, granulation loss, or monolayer disruption. Subsequently, 20 μL of MTT solution (5 mg/mL in PBS) was added to each well, and plates were incubated for 1–5 h under the same conditions. The medium was then removed, and the formazan crystals formed were dissolved in 200 μL of dimethyl sulfoxide (DMSO). After gentle shaking for 5 min at 150 rpm, absorbance was measured at 560 nm with a reference wavelength of 620 nm using a microplate reader. Cell viability was calculated as a percentage relative to untreated control cells.[31,32]

In vitro Wound-Healing (Scratch) Assay

Using the wound scratch assay, AgNP's ability to cure wounds was investigated in vitro.[33] On a 6-well culture plate, normal epithelial kidney tissue vero cells were sown, and the cells were incubated until 90% confluences. Using a sterile micropipette, the plates were scraped vertically once 90% confluence was achieved. Every well has the same amount of scratch remaining on it. After treating the cells with 150 μg/mL of AgNPs, the debris from the scratched cells was washed with fresh eagle's minimum essential medium (EMEM) (Sigma-Aldrich, St. Louis, MO, USA). After that, the cells were kept in an incubator with 5% CO_2 at 30°C for 48 hours. Following the incubation period, the wound closure was examined under a microscope, and pictures were taken. The cells' relative migration ratio (RMR) was determined using the following formula: RMR = ([A0-A1]/A0) X 100, where A0 – Area of scratch made initially, A1 – Area of scratch after 48 h incubation.

Anticoagulant Activity

The anticoagulant activity of AgNPs was evaluated using prothrombin time (PT) and activated partial thromboplastin time (APTT) assays.[34] Citrated human plasma was prepared by centrifugation of blood samples at 6000 × g for 20 min at 4 °C. Plasma samples were incubated with AgNPs at concentrations of 25, 50, and 75 μg/mL, and clotting times were measured using an automated coagulometer. Heparin-treated plasma served as the positive control for anticoagulant activity.

Statistical Analysis

All experiments were performed in independent triplicates (n = 3), and data are expressed as mean ± standard deviation (SD). Statistical analyses and graphical representations were conducted using GraphPad Prism 11.02 (San Diego, CA, USA). One-way analysis of variance (ANOVA) followed by Dunnett's multiple comparisons test was used to compare each treatment group with the control. Two-way ANOVA followed by Tukey's multiple comparisons test was applied to evaluate differences among multiple sample groups. Wound closure percentages were compared between control and treated groups using an unpaired two-tailed Student's *t*-test. Differences were considered statistically significant at $P < 0.05$. Significance thresholds were defined as: ns (not significant) > 0.05, *$P < 0.05$, **$P < 0.005$, ***$P < 0.0005$.

Results and Discussion

Isolation, Preliminary Characterization, and Molecular Identification

Bacterial colonies were obtained from seven raw milk samples, and those exhibiting morphological characteristics typical of LAB were selected for further investigation. The isolates produced small to medium-sized, circular, smooth, and creamy-white colonies on MRS agar, consistent with the colony morphology commonly reported for *Lactobacillus* species and related LAB groups cultivated on selective MRS medium. Microscopic examination revealed that the selected isolates were Gram-positive, rod-shaped, non-spore-forming bacteria, and all isolates exhibited negative catalase activity. These phenotypic characteristics are widely recognized as primary identification markers for LAB and are routinely used as preliminary screening criteria for potential probiotic strains due to the absence of cytochrome-mediated respiration systems. Similar morphological and biochemical characteristics have been reported for probiotic LAB isolated from dairy products and fermented foods.[35] In addition to morphological assessment, the isolates were quantitatively evaluated for their tolerance to acidic conditions and bile salts, which are essential physiological traits for survival in the gastrointestinal tract. The tested isolates demonstrated high resilience, maintaining a survival rate of 51.3 ± 1.2% at pH 2 and a growth efficiency of 64.7 ± 2.5% in the presence of 0.3% bile salts. These results indicate a strong potential for the isolates to withstand the harsh conditions of the stomach and upper intestine.

While tolerance to bile salts among probiotic bacteria is often hypothesized to be associated with the activity of bile salt hydrolase (BSH) enzymes—which hydrolyze conjugated bile salts to reduce toxicity and maintain membrane stability—this enzymatic mechanism was not experimentally validated in the present study and remains a subject for future investigation. Previous studies have shown that many species belonging to the genera *Lactobacillus* and *Bifidobacterium* exhibit strong bile and acid tolerance, which are considered essential functional attributes for probiotic efficacy.[36] Overall, the observed morphological, biochemical, and quantitative physiological characteristics suggest that the obtained isolates belong to lactic acid bacteria with potential probiotic properties. Based on these findings, the most promising isolate was selected for molecular identification using 16S rRNA gene sequencing.

The most promising bacterial isolate obtained from preliminary screening was subjected to molecular identification via 16S rRNA gene sequencing. The resulting sequence was deposited in the NCBI GenBank database under accession number PZ476340. BLAST analysis revealed 99.78% sequence similarity with *L. brevis* strain REVI (OQ346264) and *Lactobacillus brevis* strain NRIC 0138 (AB362619), indicating that the isolate is closely related to this species. Based on this high sequence similarity and alignment with reference strains, the isolate was identified as *L. brevis* (Figure 2). Members of *L. brevis* are widely distributed in fermented foods and dairy products and are recognized for their probiotic potential, metabolic versatility, and ability to produce bioactive metabolites. Species of the genus *Levilactobacillus* have been reported to possess probiotic attributes and metabolic capabilities relevant to nanoparticle biosynthesis, including the secretion of extracellular biomolecules capable of reducing and stabilizing metal ions. Previous studies have demonstrated that strains of *Lactobacillus* and related lactic acid bacteria can function as biological nano-factories, producing silver nanoparticles via extracellular enzymes, proteins, and polysaccharides that facilitate metal ion reduction and nanoparticle stabilization.[35,36] Consequently, the molecular identification of the isolate as *L. brevis* provides a solid foundation for its application in the biosynthesis of silver nanoparticles and the generation of biologically active nanomaterials.

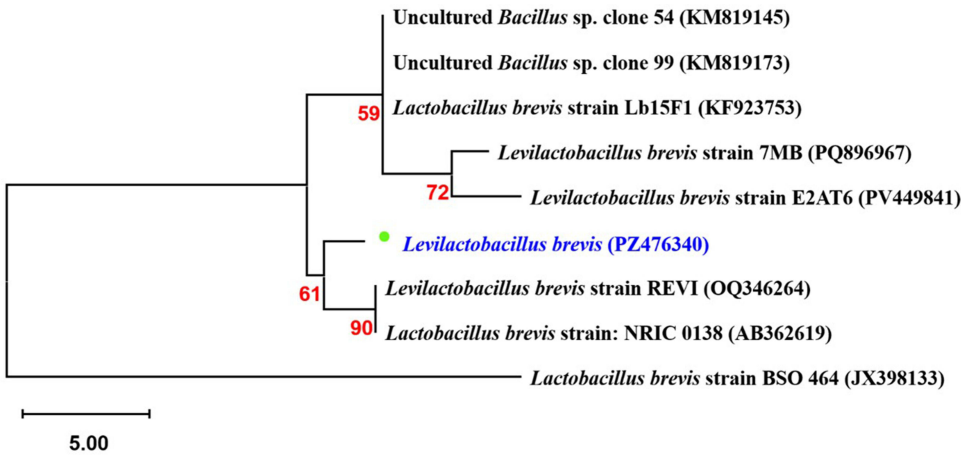

Figure 2 Maximum-likelihood phylogenetic tree based on 16S rRNA gene sequences showing the relationship of the isolate (*Levilactobacillus brevis* PZ476340) to closely related reference strains. Bootstrap values (%) are shown at branch nodes; the scale bar indicates nucleotide substitutions per site.

Biosynthesis of Silver Nanoparticles by L. brevis

The biosynthesis of AgNPs was carried out using the cell-free culture supernatant of the identified probiotic strain *L. brevis* as a biological reducing and stabilizing agent. Formation of AgNPs was initially confirmed through visual observation of a distinct color change in the reaction mixture after the addition of $AgNO_3$ solution. The reaction mixture gradually changed from pale yellow to dark brown during incubation, indicating the reduction of silver ions (Ag^+) into metallic silver nanoparticles (Ag^0), which is a typical visual indicator of nanoparticle formation. This color transition is commonly associated with the excitation of SPR in AgNPs. Similar color changes have been reported in numerous studies involving the biological synthesis of silver nanoparticles using microbial culture filtrates and plant extracts.[37] The visual confirmation of nanoparticle formation suggests that biomolecules present in the extracellular culture filtrate of *L. brevis* played a key role in the bioreduction process. These biomolecules may include proteins, enzymes, polysaccharides, and other secondary metabolites secreted during bacterial growth. Such compounds can function simultaneously as reducing agents, converting Ag^+ ions to metallic silver, and as capping agents, stabilizing the newly formed nanoparticles and preventing their aggregation. Microbial-mediated nanoparticle synthesis is considered an environmentally friendly alternative to conventional chemical and physical methods because it occurs under mild reaction conditions without the need for toxic reducing agents or high-energy processes. Lactic acid bacteria, including species of *Lactobacillus*, have been reported to facilitate nanoparticle biosynthesis through extracellular enzymatic systems and biomolecular interactions that promote metal ion reduction.[30] Silver nanoparticles were successfully biosynthesized using the probiotic bacterium *Lactobacillus acidophilus*.[38] The use of a well-characterized probiotic strain offers advantages in terms of safety and potential co-delivery applications, which may enhance therapeutic efficacy and confer synergistic health benefits.[30–32] The successful formation of AgNPs by *L. brevis* therefore demonstrates the potential of probiotic bacteria to function as biological nano-factories, capable of producing metallic nanoparticles through sustainable and eco-friendly processes. Following the visual confirmation of nanoparticle formation, the synthesized AgNPs were purified and subjected to detailed physicochemical characterization using spectroscopic and microscopic techniques.

Physicochemical Characterization of Biosynthesized AgNPs

Following visual confirmation of nanoparticle formation, the biosynthesized AgNPs were subjected to comprehensive physicochemical characterization to determine their optical properties, structural features, morphology, and colloidal stability. Characterization of nanoparticles is essential to verify successful synthesis and to understand the physicochemical parameters that govern their biological activity. In the present study, multiple complementary analytical techniques—including UV–Vis spectroscopy, FTIR, TEM, and zeta potential analysis—were employed to provide a rigorous assessment of nanoparticle size distribution, surface chemistry, and stability.

UV-Visible Spectroscopy Analysis

The formation and optical properties of the biosynthesized AgNPs were initially assessed using UV–Vis spectroscopy. The absorption spectrum of the nanoparticle suspension exhibited a distinct SPR peak at approximately 410 nm, characteristic of metallic silver nanoparticles. This SPR band arises from localized surface plasmon resonance (LSPR), in which conduction electrons on the nanoparticle surface undergo collective oscillations upon excitation by incident light. Typically, AgNPs exhibit absorption peaks between 400 and 500 nm due to SPR.[39] Similar observations have been reported in previous studies. For instance, Syame et al,[40] reported a SPR peak at 410 nm for AgNPs synthesized using the cell-free supernatant of *Lactobacillus plantarum* and *Lactobacillus brevis*, and Naseer et al,[5] observed a clear peak at 410 nm for AgNPs produced by *Lactobacillus bulgaricus* The presence of a single, asymmetrical SPR peak near 410 nm provides preliminary insights into the physical properties of the nanoparticles. The symmetry of the peak suggests that the synthesized AgNPs are predominantly spherical, as non-spherical geometries (eg, rods or prisms) typically produce multiple resonant bands due to anisotropic electron oscillations. While the peak position aligns with literature values for well-dispersed spherical AgNPs below 50 nm,[41,42] the broader baseline and tailing of the absorption curve indicate a degree of polydispersity and the potential presence of minor nanoparticle aggregates. Because the position, intensity, and full-width at half-maximum (FWHM) of the SPR band are highly sensitive to nanoparticle size, shape, and local refractive index, these spectroscopic data were corroborated with high-resolution imaging to validate the dispersion state and size distribution of the synthesized AgNPs.

FTIR and TEM Analysis

FTIR spectroscopy was performed to identify the functional groups associated with the biosynthesized nanoparticles and to elucidate the specific biomolecules involved in the reduction of silver ions and subsequent surface passivation. The FTIR spectrum of the purified AgNPs (Figure 3) displayed a complex profile of absorption bands, reflecting a multi-component organic capping layer derived from the *L. brevis* culture filtrate. The prominent peak at 1633 cm^{-1} (Amide I) strongly indicates that extracellular proteins secreted by *L. brevis* are structurally associated with the nanoparticles, likely interacting through amine or cysteine residues to form a stabilizing envelope. Additional peaks in the 1500–1200 cm^{-1} region correspond to C–N stretching and N–H bending modes of aliphatic amines, further confirming the proteinaceous nature of the capping matrix. Furthermore, the absorption band near ~1050 cm^{-1} is assigned to the C–O stretching vibrations of carbohydrates, implying that extracellular polysaccharides (EPS) or glycolipids co-adsorb onto the nanoparticle surface.

TEM and selected area electron diffraction (SAED) analyses were performed to evaluate the morphology, size distribution, and crystalline structure of the biosynthesized silver nanoparticles. As shown in the TEM micrograph (Figure 4A), the nanoparticles were predominantly spherical and exhibited a size range of 7–55 nm, with an average diameter of 27.18 ± 12.7 nm, as determined from the particle size distribution histogram (Figure 5). The nanoscale dimensions of the synthesized AgNPs provide a high surface-area-to-volume ratio, which may contribute to enhanced biological activity. Although the nanoparticles were generally well dispersed, small clusters were observed in some regions of the micrographs, indicating a tendency toward aggregation during sample drying or under vacuum conditions. Such aggregation may result from interactions between biomolecular capping agents associated with the nanoparticle surface. The crystalline nature of the synthesized AgNPs was confirmed by the SAED pattern (Figure 4B), which displayed distinct concentric diffraction rings corresponding to the characteristic planes of face-centered cubic (fcc) metallic silver. These findings demonstrate that the extracellular metabolites of *L. brevis* effectively mediated nanoparticle nucleation and crystal growth, resulting in highly crystalline nanostructures. Comparable results have been reported by Syame et al,[40] who synthesized AgNPs using the cell-free supernatants of *Lactobacillus plantarum* and *L. brevis* The resulting nanoparticles were predominantly spherical to polyhedral, polydispersed, and ranged from 5 to 40 nm in diameter, which is consistent with the size distribution observed in the present study.

Zeta Potential Analysis and Stability Assessment

The surface charge and colloidal stability of the biosynthesized silver nanoparticles were evaluated by zeta potential analysis, and the resulting profile is presented in Figure 6. The synthesized AgNPs exhibited an average zeta potential of

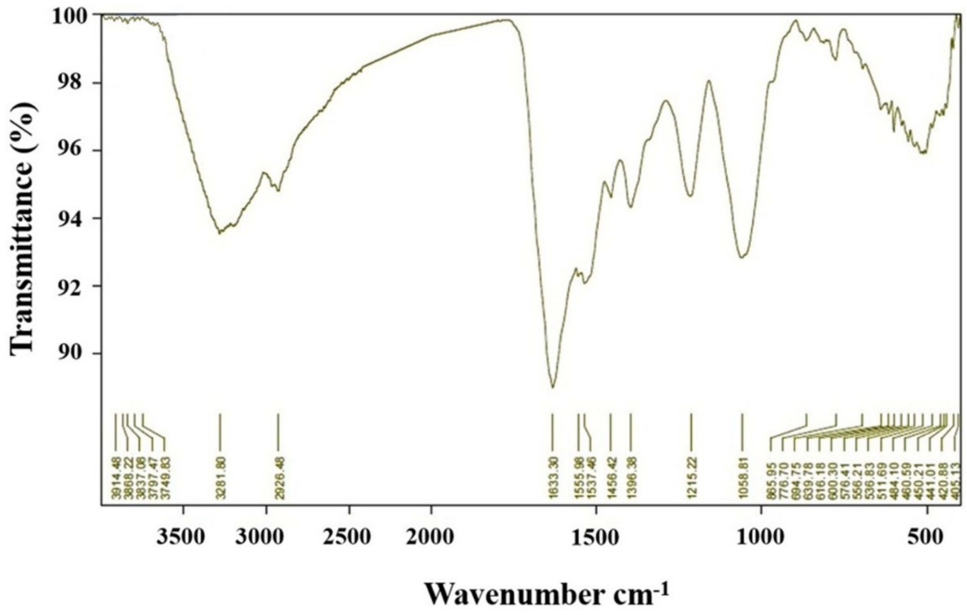

Figure 3 Fourier-transform infrared (FTIR) spectrum of biosynthesized silver nanoparticles (AgNPs) produced by *Levilactobacillus brevis*. The spectrum shows characteristic absorption bands corresponding to hydroxyl, amine, carbonyl, and polysaccharide-associated functional groups, indicating the involvement of extracellular biomolecules in the reduction, capping, and stabilization of AgNPs.

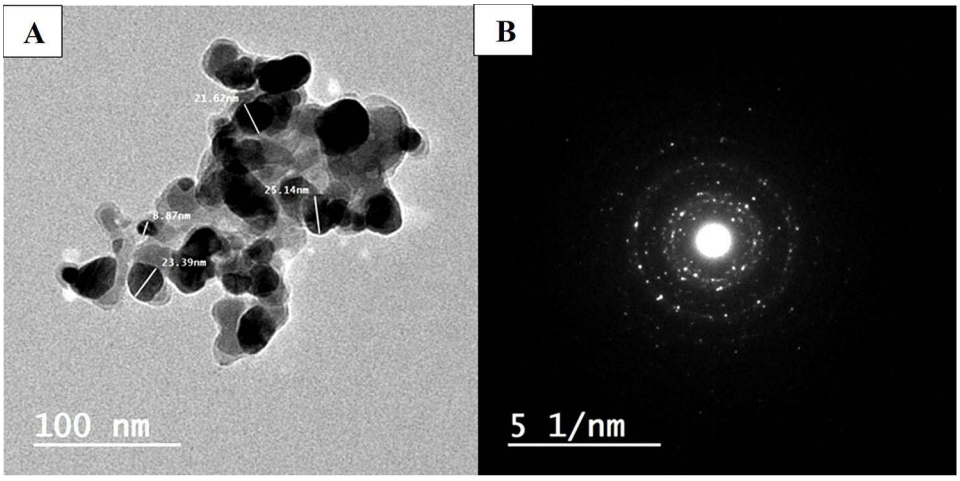

Figure 4 Transmission electron microscopy (TEM) and selected area electron diffraction (SAED) analyses of biosynthesized silver nanoparticles (AgNPs) produced by *Levilactobacillus brevis*. (**A**) TEM micrograph showing predominantly spherical AgNPs with nanoscale dimensions and localized aggregation. (**B**) SAED pattern displaying characteristic diffraction rings, confirming the crystalline nature of the nanoparticles and the formation of a face-centered cubic (fcc) silver structure.

−2.57 mV, indicating a weak negative surface charge. The negative zeta potential suggests that the nanoparticle surface was coated with negatively charged biomolecules derived from the extracellular metabolites of *L. brevis*. These biomolecules, including proteins, amino acids, and polysaccharides, likely adsorbed onto the nanoparticle surface during biosynthesis and acted as capping agents. FTIR analysis further supported the presence of these surface-associated biomolecules. Surface charge is an important factor influencing the colloidal stability of nanoparticle suspensions. In general, nanoparticles with absolute zeta potential values greater than ±30 mV are considered highly stable due to strong electrostatic repulsion that minimizes particle aggregation. In the present study, the relatively low zeta potential value indicates limited electrostatic stabilization. However, biologically synthesized nanoparticles frequently exhibit lower zeta potential values because their stability is often maintained by steric hindrance provided by adsorbed biomolecules rather than by electrostatic repulsion alone. Therefore, the colloidal behavior of the synthesized AgNPs is likely governed

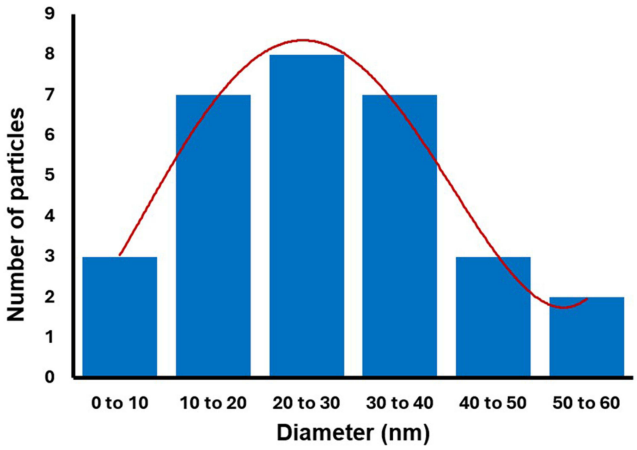

Figure 5 Particle size distribution histogram of biosynthesized silver nanoparticles (AgNPs) produced by *Levilactobacillus brevis*, as determined from TEM measurements. The nanoparticles exhibited a size range of 7–55 nm with an average diameter of 27.18 ± 12.7 nm, indicating a predominantly nanoscale and moderately polydisperse population.

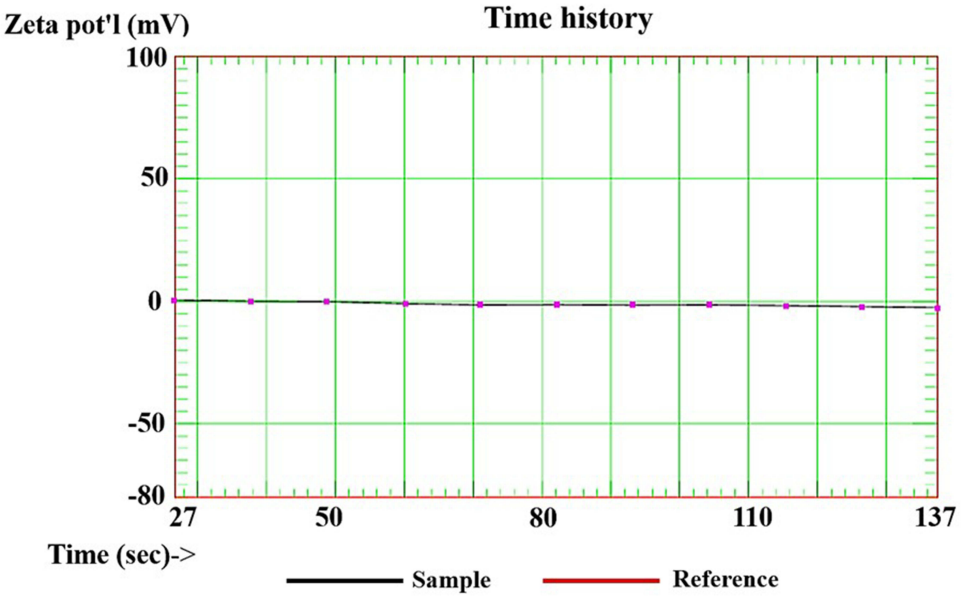

Figure 6 Zeta potential analysis of biosynthesized silver nanoparticles (AgNPs) produced by *Levilactobacillus brevis*, showing an average surface charge of −2.57 mV and the presence of a weakly negative biomolecule-capped nanoparticle surface.

primarily by steric stabilization arising from the biomolecular capping layer produced by *L. brevis*. Similar negative zeta potential values have been reported for microbial- and plant-mediated silver nanoparticles, where proteins and polysaccharides associated with the nanoparticle surface contribute significantly to colloidal stability and resistance to aggregation.[36] Overall, the zeta potential and FTIR results collectively indicate that the synthesized AgNPs possess a negatively charged, biomolecule-capped surface that contributes to their colloidal stability.

Biological Activities of Biosynthesized AgNPs

Following physicochemical characterization, the biological activities of the biosynthesized silver nanoparticles were evaluated to assess their potential biomedical applications. Nanoparticles synthesized through biological routes often exhibit enhanced biological functionality due to the presence of surface-bound biomolecules that can influence cellular interactions and redox behavior. In the present study, the biological performance of the AgNPs produced by *L. brevis* was investigated through several in vitro assays, including antioxidant activity, cytotoxic and anticancer evaluation, wound-

https://doi.org/10.2147/IJN.S612998

healing potential, and anticoagulant effects. These analyses provide important insight into the possible therapeutic applications of the biosynthesized nanoparticles.

Antioxidant Activity of Biosynthesized AgNPs

The antioxidant activity of the biosynthesized silver nanoparticles was evaluated using the DPPH radical scavenging assay. As shown in Figure 7, the AgNPs exhibited concentration-dependent antioxidant activity, with radical scavenging increasing progressively as nanoparticle concentration increased. The highest scavenging activity (79.7%) was observed at 1000 μg/mL, whereas the lowest concentration tested (1.95 μg/mL) exhibited approximately 20.1% scavenging activity. No radical scavenging activity was detected in the control group. The calculated IC_{50} value was 61.4 μg/mL, indicating considerable antioxidant potential. Statistical analysis revealed highly significant differences among the tested concentrations [F (6,14) = 9581, $P < 0.0001$]. Dunnett's multiple comparisons test demonstrated significant differences between all treatment groups and the control ($P < 0.0001$), while the Brown–Forsythe test confirmed homogeneity of variance among groups ($P = 0.9132$). The observed antioxidant activity may be attributed to the synergistic effects of the metallic silver core and the biomolecular capping agents associated with the nanoparticle surface. FTIR analysis revealed the presence of hydroxyl, amine, and carbonyl-containing functional groups derived from extracellular proteins, enzymes, and polysaccharides produced by *L. brevis*. These biomolecules may contribute to free-radical scavenging through electron or hydrogen donation mechanisms. In addition, AgNPs have been reported to exhibit intrinsic antioxidant properties and enzyme-mimetic activities, including catalase-like decomposition of hydrogen peroxide, which may further contribute to their antioxidant performance.[43,44] The nanoscale dimensions of the synthesized AgNPs (7–55 nm) may also enhance antioxidant activity by increasing the available surface area for interaction with reactive oxygen species (ROS). Similar concentration-dependent antioxidant activities have been reported for AgNPs biosynthesized using probiotic bacteria, including *Lactobacillus gasseri, Lactobacillus plantarum*, and *Ligilactobacillus salivarius*, as well as other microbial and plant-mediated synthesis systems.[45,46] The antioxidant activity observed in the present study is comparable to previously reported values and highlights the potential of *L. brevis*-derived AgNPs as bioactive nanomaterials for applications involving oxidative stress-related disorders. Overall, the results demonstrate that the biosynthesized AgNPs possess significant antioxidant activity, supporting their potential application in biomedical and pharmaceutical fields.

Cytotoxic and Anticancer Activity of Biosynthesized AgNPs

The cytotoxic and anticancer activities of the biosynthesized silver nanoparticles were evaluated using the MTT assay, which measures cellular metabolic activity as an indicator of cell viability. In this assay, metabolically active cells reduce the tetrazolium salt MTT into insoluble formazan crystals, and the intensity of the developed color is proportional to the number of viable cells. The assay was performed using Vero normal kidney epithelial cells, MCF-7 breast cancer cells, and HepG2 liver carcinoma cells exposed to different concentrations of AgNPs. As shown in Figure 8A, the synthesized

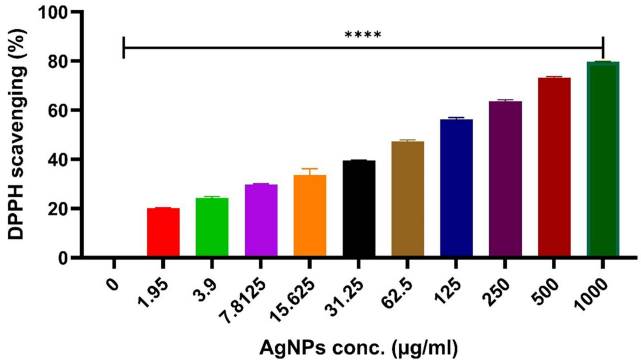

Figure 7 DPPH radical scavenging activity of biosynthesized silver nanoparticles (AgNPs) produced by *Levilactobacillus brevis* at different concentrations (1.95–1000 μg/mL). The AgNPs exhibited a concentration-dependent increase in antioxidant activity, reaching 79.7% scavenging at 1000 μg/mL. Data are presented as mean ± SD (n = 3). Statistical significance was determined by one-way ANOVA followed by Dunnett's multiple comparisons test (****$P < 0.0001$ vs control).

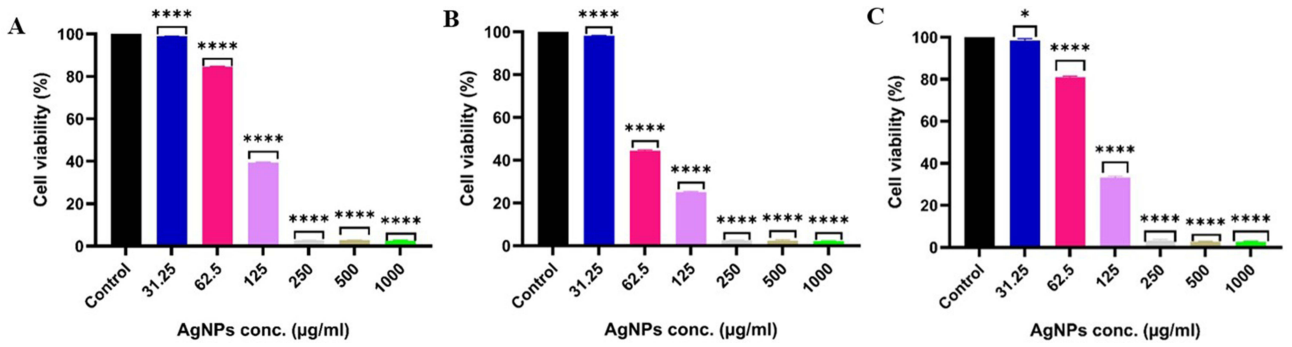

Figure 8 Cytotoxic effects of biosynthesized silver nanoparticles (AgNPs) produced by *Levilactobacillus brevis* on (**A**) Vero normal kidney epithelial cells, (**B**) MCF-7 human breast cancer cells, and (**C**) HepG2 human hepatocellular carcinoma cells, as determined by the MTT assay after treatment with different AgNP concentrations (31.25–1000 µg/mL). Cell viability decreased in a concentration-dependent manner, with MCF-7 cells exhibiting the highest sensitivity to AgNP treatment. Data are presented as mean ± SD (n = 3). Statistical significance was determined by one-way ANOVA followed by Dunnett's multiple comparisons test. *$P < 0.05$ and ****$P < 0.0001$ versus the untreated control.

AgNPs exhibited a clear concentration-dependent cytotoxic effect against Vero cells. Cell viability decreased markedly with increasing nanoparticle concentration, reaching 2.48%, 2.79%, and 2.73% at 1000, 500, and 250 µg/mL, respectively. In contrast, lower concentrations showed reduced cytotoxicity, with cell viability values of 39.26%, 84.57%, and 98.88% at 125, 62.5, and 31.25 µg/mL, respectively. The IC_{50} value against Vero cells was 110.29 µg/mL. A stronger cytotoxic effect was observed against MCF-7 breast cancer cells (Figure 8B). Cell viability was reduced to 2.21%, 2.35%, and 2.57% at 1000, 500, and 250 µg/mL, respectively. At lower concentrations, viability increased to 25.1%, 44.43%, and 98.42% at 125, 62.5, and 31.25 µg/mL, respectively, with an IC_{50} value of 81.28 µg/mL. These results indicate that the AgNPs showed greater cytotoxicity toward MCF-7 cells than toward Vero cells. Similarly, HepG2 cells showed concentration-dependent sensitivity to the biosynthesized AgNPs (Figure 8C). Cell viability decreased to 3.15%, 2.77%, and 2.53% at 250, 500, and 1000 µg/mL, respectively. At lower concentrations, viability increased to 33.33%, 81.04%, and 98.38% at 125, 62.5, and 31.25 µg/mL, respectively. The IC_{50} value against HepG2 cells was 102.64 µg/mL. One-way ANOVA revealed highly significant differences among the tested concentrations in all cell lines: Vero cells [$F(6,14) = 1464$, $P < 0.0001$], MCF-7 cells [$F(6,14) = 67114$, $P < 0.0001$], and HepG2 cells [$F(6,14) = 20910$, $P < 0.0001$]. Dunnett's multiple comparisons test showed significant differences between all AgNP-treated groups and their corresponding controls ($P < 0.0001$), except for the comparison between the control and the lowest concentration of AgNPs in HepG2 cells (31.25 µg/mL; $P = 0.0134$). These findings confirm the dose-dependent cytotoxic behavior of the biosynthesized AgNPs.

The cytotoxic activity of AgNPs has been widely attributed to several mechanisms, particularly ROS generation, mitochondrial dysfunction, DNA damage, and activation of apoptotic pathways. Owing to their nanoscale dimensions and high surface reactivity, AgNPs can interact with cellular membranes and intracellular components, including proteins, lipids, and nucleic acids, leading to oxidative stress and impaired metabolic activity. Excessive ROS production may induce lipid peroxidation, protein oxidation, and DNA strand damage.[39,47] Furthermore, AgNP-induced oxidative stress can disrupt mitochondrial membrane potential, promote cytochrome c release, activate caspase-mediated apoptosis, and stimulate stress-responsive proteins such as p53, thereby contributing to cell cycle arrest and inhibition of cell proliferation.[48] The observed cytotoxicity may also be associated with the small size of the synthesized nanoparticles, which ranged from 7 to 55 nm according to TEM analysis. Nanoparticles within this size range possess a high surface-area-to-volume ratio, which enhances cellular uptake and increases nanoparticle–cell interactions. Increased intracellular accumulation of AgNPs may intensify oxidative stress and promote cytotoxic responses. Similar concentration-dependent cytotoxic effects have been reported for biosynthesized AgNPs in different cancer cell lines, supporting their potential use in anticancer and nanotherapeutic applications.[49] Several previous studies support the present findings. Mohammed et al,[50] reported that AgNPs produced by *Lactobacillus acidophilus* exhibited cytotoxicity against Caco, A549, and HepG2 cancer cell lines, with half-maximal response concentrations of 5, 15, and 30 mg/mL, respectively Similarly, AgNPs synthesized using *Lactobacillus salivarius* showed cytotoxic activity against MCF-7 breast cancer cells, with an

https://doi.org/10.2147/IJN.S612998

IC_{50} value of 52.29 µg/mL, indicating their potential as anticancer agents.[51] Devi and Bhimba[52] evaluated the anticancer activity of AgNPs against Hep-2, MCF-7, HT29, and Vero cell lines and reported that AgNPs reduced cell viability in a concentration-dependent manner. Inbathmizh et al,[53] also showed that biosynthesized AgNPs reduced HepG2 cell viability at high concentrations.

Recent studies further confirm the anticancer potential of biologically synthesized AgNPs. Siddiqui et al,[54] demonstrated that AgNPs derived from the probiotic strain *Lactobacillus casei* exhibited anticancer and anti-metastatic activities by inhibiting migration and invasion of A-549 human lung cancer cells Ravi et al,[55] reported that chitosan-encapsulated AgNPs synthesized using probiotic *Lactobacillus plantarum* showed dose-dependent cytotoxicity against HeLa cervical cancer cells, with an IC_{50} value of approximately 2673 ± 1.911 µg/mL after 24 h. Yuksekdag et al,[56] found that AgNPs synthesized using *Ligilactobacillus salivarius* were non-toxic to L929 normal cells at low concentrations (039–25 µg/mL), while higher concentrations produced measurable cytotoxic effects, with IC_{50} values of 113, 117, and 162 µg/mL after 24, 48, and 72 h, respectively. Biogenic AgNPs have also been reported to overcome multidrug resistance in cancer cells. For example, AgNPs synthesized using fungal extracts such as *Aspergillus niger* were shown to disrupt efflux pump activity in resistant breast cancer cells (MCF-7/ADR), thereby enhancing intracellular accumulation of chemotherapeutic agents such as doxorubicin.[57] Moreover, the biocompatibility of biogenic AgNPs is often attributed to natural capping agents, including polyphenols, flavonoids, proteins, and polysaccharides, which may reduce toxicity toward normal cells compared with chemically synthesized nanoparticles.[58]

Additional plant- and microbe-mediated AgNPs have shown comparable anticancer effects. Ali et al,[59] reported a concentration-dependent cytotoxic effect of *Fusarium equiseti*-derived AgNPs against MCF-7 breast cancer cells, with an IC_{50} value of 2438 µg/mL. Al-Janabi et al,[60] demonstrated that AgNPs synthesized using a glycolipopeptide biosurfactant produced by *Lactobacillus plantarum* inhibited MCF-7 breast cancer cells by 5477% at 400 µg/mL. Nguyen et al,[61] reported that AgNPs synthesized using *Callisia fragrans* leaf extract exhibited anticancer activity against MCF-7, HepG2, KB, LU-1, and MKN-7 cell lines, with IC_{50} values of 241, 2.31, 2.65, 3.26, and 2.40 µg/mL, respectively. Al Baloushi et al,[62] also reported anticancer activity of *Moringa peregrina*-derived AgNPs against MCF-7 cells, with an IC_{50} value of 2693 µg/mL. The cytotoxic effects of the biosynthesized AgNPs were further supported by microscopic examination of Vero, MCF-7, and HepG2 cells after treatment with increasing nanoparticle concentrations (Figures 9–11). Untreated control cells showed normal morphology, high cell density, and intact monolayer organization. In contrast, AgNP-treated cells exhibited concentration-dependent morphological alterations consistent with progressive cellular damage and reduced viability. In Vero cells (Figure 9), AgNP treatment caused a gradual reduction in cellular confluence and disruption of monolayer integrity. Cells exposed to higher concentrations (250–1000 µg/mL) showed marked morphological deterioration, including cell shrinkage, rounding, irregular distribution, and extensive detachment from the culture surface. At 125 µg/mL, partial cellular damage and reduced proliferation were observed, whereas cells treated with lower concentrations (31.25–62.5 µg/mL) largely retained normal morphology and adherence, although a modest reduction in cell density was still evident.

A more pronounced response was observed in the cancer cell lines. MCF-7 cells (Figure 10) showed extensive loss of confluence and disruption of monolayer architecture at concentrations ≥250 µg/mL, accompanied by cell shrinkage, fragmentation, and detachment. These observations are consistent with previous reports showing that AgNPs exert cytotoxic and apoptotic effects against MCF-7 cells by damaging membrane integrity and inducing nuclear fragmentation through ROS-mediated oxidative stress.[63] Similar growth inhibitory effects of green AgNPs against MCF-7 cells have also been reported by Chahardoli et al,[64] Abdel-Rahman et al,[65] further demonstrated significant cytotoxic effects of biogenic AgNPs against HepG2 and MCF-7 cells Likewise, HepG2 cells (Figure 11) exhibited severe morphological disruption at higher AgNP concentrations, including reduced cell density, loss of cell-to-cell interactions, and extensive cellular detachment. At intermediate concentrations, both cancer cell lines displayed noticeable alterations in morphology and adherence, whereas lower concentrations produced comparatively milder effects. These morphological changes are characteristic of AgNP-induced cytotoxicity and are consistent with apoptosis-associated cellular responses, including membrane damage, cytoskeletal disruption, loss of adhesion, and cellular shrinkage. In agreement with these findings, Ahsan et al,[66] reported that AgNPs synthesized using *Parthenium hysterophorus* leaf extract significantly reduced HepG2 cell viability, with cell survival decreasing below 65% after 24 h even at low concentrations and reaching approximately

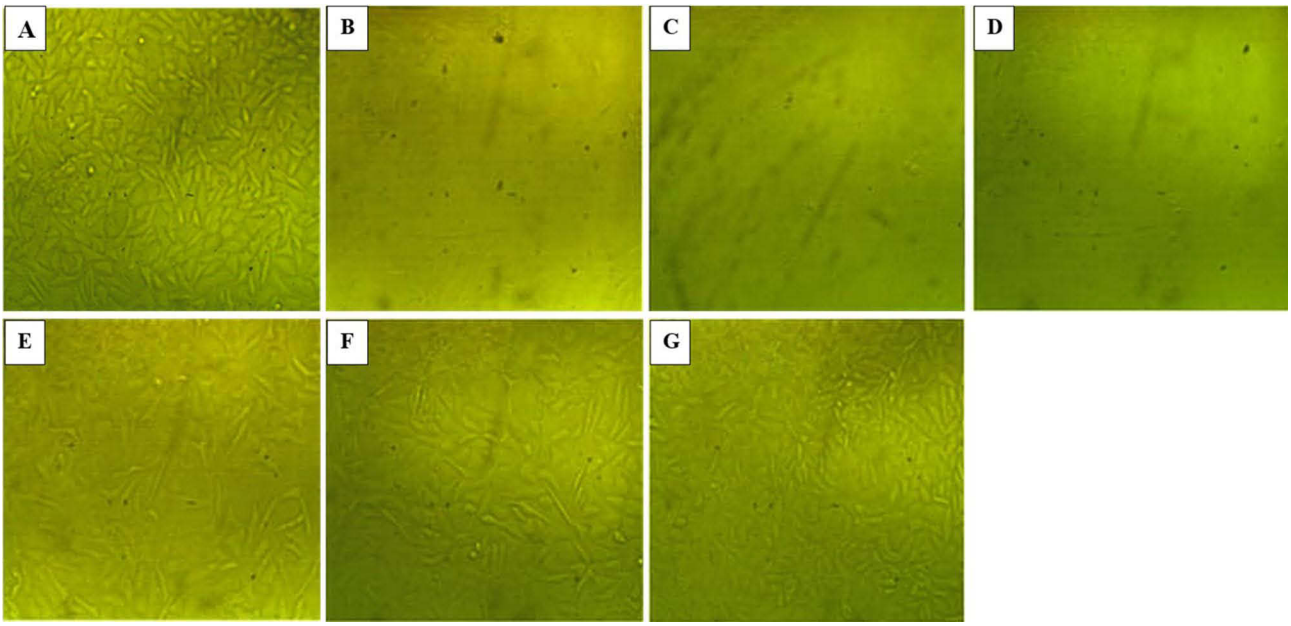

Figure 9 Representative photomicrographs showing the morphological changes of Vero cells following treatment with biosynthesized silver nanoparticles (AgNPs) at different concentrations: (**A**) untreated control, (**B**) 1000 μg/mL, (**C**) 500 μg/mL, (**D**) 250 μg/mL, (**E**) 125 μg/mL, (**F**) 62.5 μg/mL, and (**G**) 31.25 μg/mL. AgNP treatment induced concentration-dependent morphological alterations, including reduced cellular confluence, cell shrinkage, rounding, and detachment, indicative of cytotoxic effects compared with the untreated control.

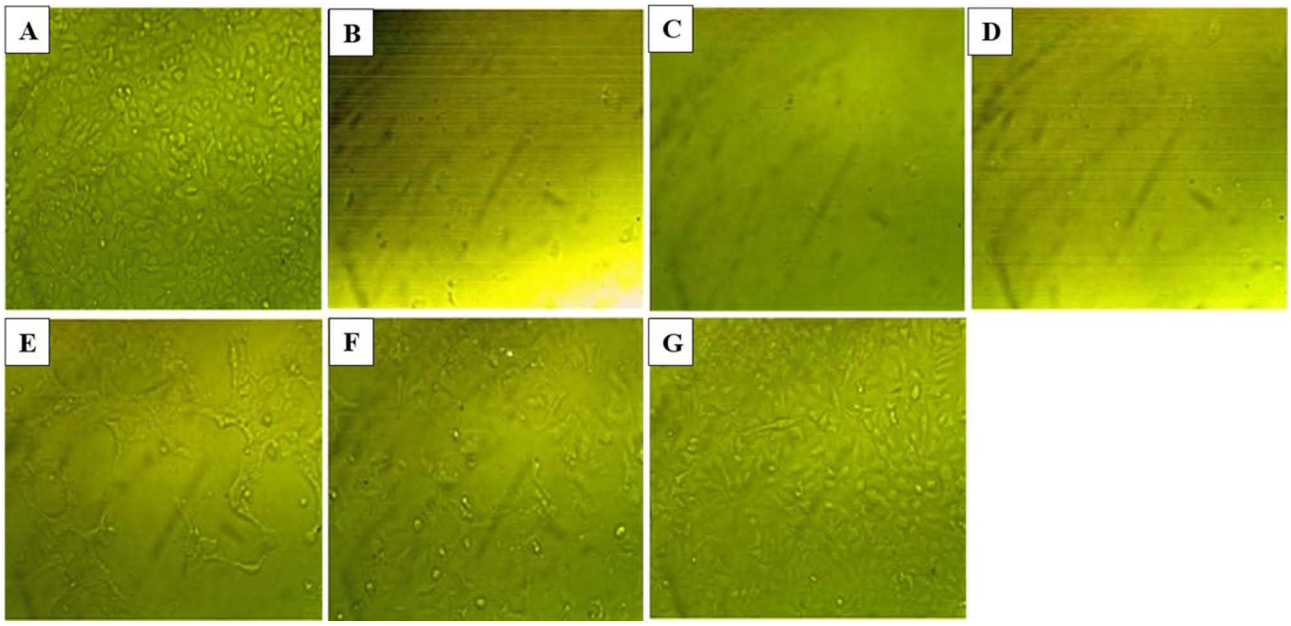

Figure 10 Representative photomicrographs showing the morphological changes of MCF-7 breast cancer cells following treatment with biosynthesized silver nanoparticles (AgNPs) at different concentrations: (**A**) untreated control, (**B**) 1000 μg/mL, (**C**) 500 μg/mL, (**D**) 250 μg/mL, (**E**) 125 μg/mL, (**F**) 62.5 μg/mL, and (**G**) 31.25 μg/mL. AgNP treatment induced concentration-dependent morphological alterations, including loss of cellular confluence, disruption of monolayer architecture, cell shrinkage, fragmentation, and detachment, particularly at concentrations ≥250 μg/mL. Cells treated with lower concentrations (31.25–62.5 μg/mL) largely retained their normal morphology and adherence.

1254% at higher concentrations. Importantly, the microscopic observations closely paralleled the MTT assay results (Figure 8), confirming a concentration-dependent reduction in cell viability across all tested cell lines. The stronger morphological deterioration and lower IC_{50} value observed in MCF-7 cells compared with Vero cells suggest a relatively higher antiproliferative effect against cancer cells. Collectively, these quantitative and qualitative findings demonstrate

https://doi.org/10.2147/IJN.S612998

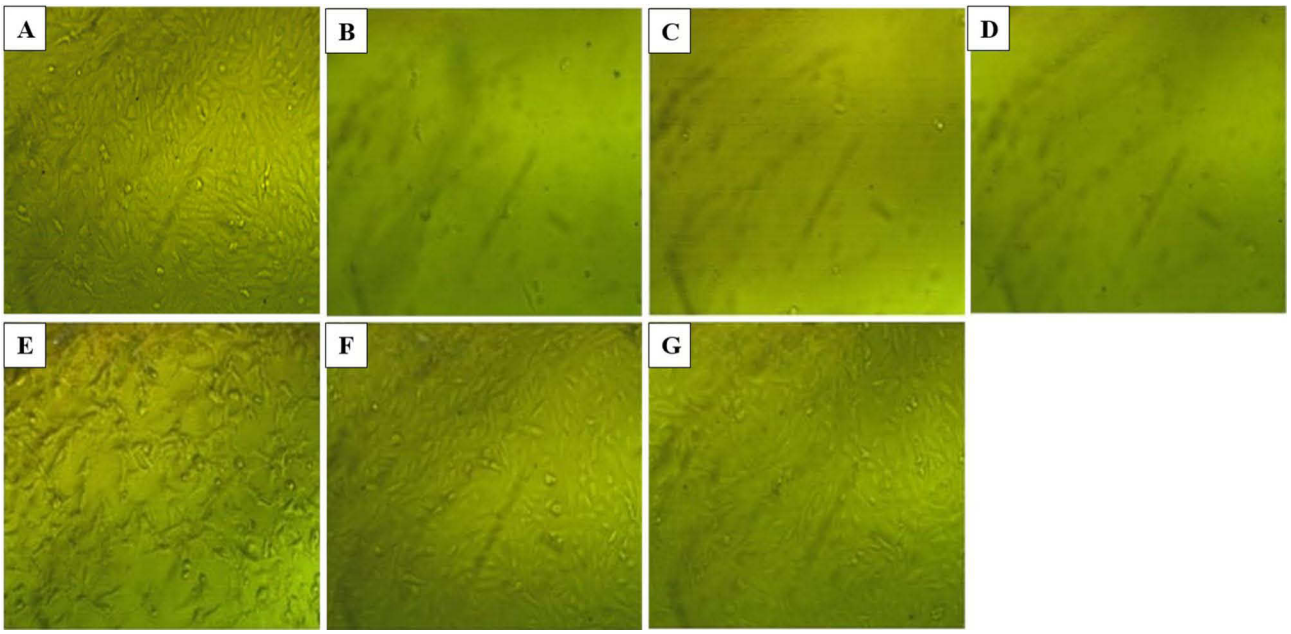

Figure 11 Representative photomicrographs showing the morphological changes of HepG2 human hepatocellular carcinoma cells following treatment with biosynthesized silver nanoparticles (AgNPs) at different concentrations: (**A**) untreated control, (**B**) 1000 μg/mL, (**C**) 500 μg/mL, (**D**) 250 μg/mL, (**E**) 125 μg/mL, (**F**) 62.5 μg/mL, and (**G**) 31.25 μg/mL. AgNP treatment induced concentration-dependent morphological alterations, including reduced cellular confluence, loss of cell-to-cell interactions, cellular shrinkage, and detachment, particularly at concentrations ≥250 μg/mL. Cells exposed to lower concentrations (31.25–62.5 μg/mL) retained relatively normal morphology with only minor changes in cell density and adherence.

that AgNPs synthesized by *L. brevis* exhibit potent cytotoxic and anticancer activities, supporting their potential application as multifunctional biogenic nanomaterials.

Overall, the results demonstrate that the biosynthesized AgNPs produced by *L. brevis* possess significant concentration-dependent cytotoxic and anticancer activities against MCF-7 and HepG2 cells, while exhibiting comparatively lower toxicity toward normal Vero cells. The observed reduction in cell viability, together with the pronounced morphological alterations, supports the involvement of oxidative stress-mediated cellular damage and apoptosis in the mechanism of action of the nanoparticles. The enhanced biological activity may be attributed to the combined effects of their nanoscale dimensions, high surface reactivity, crystalline structure, and biomolecular capping layer derived from *L. brevis* metabolites. These findings highlight the potential of probiotic-mediated AgNPs as multifunctional nanomaterials for cancer-related biomedical applications and warrant further investigation into their molecular mechanisms, selectivity, and in vivo therapeutic efficacy.

Wound-Healing Activity of Biosynthesized AgNPs

The wound-healing potential of the biosynthesized AgNPs was evaluated using an in vitro scratch assay, a standard method for assessing cell migration and proliferation during tissue repair. In this assay, a linear scratch was introduced into a confluent monolayer of Vero cells to simulate a wound, and cell migration into the scratched area was monitored over time. The results are shown in Figure 12, with quantitative measurements of wound area and width summarized in Table 1. At the initial time point (0 h), the wound area exhibited a clear gap between the cell layers. In the untreated control group, natural cell migration and proliferation led to a progressive decrease in wound area, resulting in 64.37% closure after 48 h. In contrast, AgNP-treated cells displayed a moderate wound-healing response. Limited migration was observed after 24 h, corresponding to ~5% closure (Figure 12A), while wound closure increased to 34.53% after 48 h (Figure 12B). The difference between the control and AgNP-treated groups at 48 h was statistically significant (unpaired *t*-test, $t = 3.698$, $df = 10$, $P = 0.004$). Table 1 shows that the mean wound area in AgNP-treated cells decreased from 771.66 μm^2 at 0 h to 505.16 μm^2 after 48 h. The reduced wound-closure rate in AgNP-treated cells compared with controls may be related to cytotoxic effects at the tested concentration, as demonstrated in the MTT assay. High

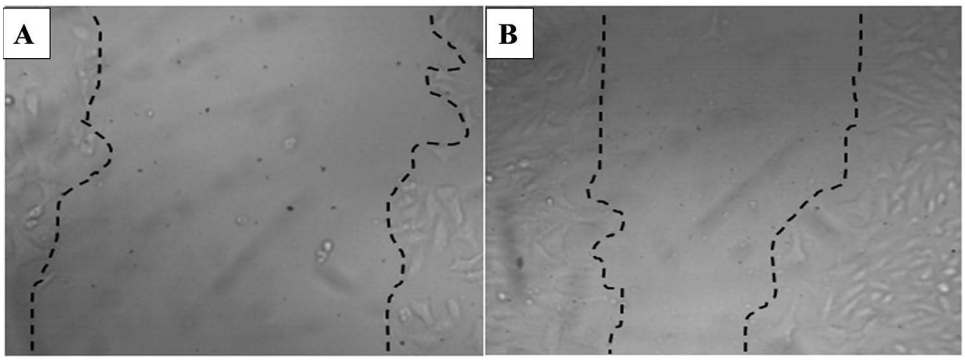

Figure 12 In vitro scratch wound-healing assay of Vero cells treated with biosynthesized silver nanoparticles (AgNPs). Representative micrographs showing cell migration into the scratched area after (**A**) 24 h and (**B**) 48 h of treatment. Dashed lines indicate the wound boundaries. Progressive closure of the wound area was observed over time, corresponding to approximately 5% and 34.53% wound closure after 24 h and 48 h, respectively.

concentrations of AgNPs can induce oxidative stress and impair cellular metabolic activity, partially inhibiting proliferation and migration. Nevertheless, the progressive decrease in wound area indicates that biosynthesized AgNPs still permit partial cell migration and tissue repair. AgNPs are known to influence wound-healing processes through several mechanisms, including modulation of inflammatory responses, stimulation of fibroblast activity, and antimicrobial effects that prevent infection at wound sites.[18] The relatively small size of the synthesized nanoparticles (10–25 nm, TEM analysis) may enhance interactions with cellular membranes and extracellular molecules, influencing migration behavior. Biologically synthesized AgNPs have previously been reported to promote wound healing by stimulating fibroblast proliferation and modulating oxidative stress.[46] Several studies support these observations. Ravi et al,[55] reported that chitosan-encapsulated AgNPs produced using *Lactobacillus plantarum* exhibited anti-proliferative effects on HeLa cells, partially inhibiting cell migration Such anti-wound healing effects are attributed to the nanoparticles' ability to suppress epithelial–mesenchymal transition (EMT), downregulate N-cadherin and vimentin, and upregulate E-cadherin, thereby inhibiting cell invasiveness.[67,68] Conversely, AgNPs synthesized from probiotic *Lactiplantibacillus plantarum* demonstrated strong wound-healing activity, with 96% closure observed in fibroblast cells at non-cytotoxic concentrations.[69] Overall, these findings indicate that the biosynthesized AgNPs exhibit moderate wound-healing activity, with measurable cell migration over time despite cytotoxic effects at higher concentrations. The results suggest that the biological activity of AgNPs is strongly dose-dependent: lower or optimized concentrations may support tissue repair, whereas higher concentrations exert cytotoxic effects.

Anticoagulant Activity of Biosynthesized AgNPs

The anticoagulant activity of the biosynthesized AgNPs was evaluated using PT and APTT assays, which assess the extrinsic and intrinsic coagulation pathways, respectively. The effects of different AgNP concentrations on clotting time were compared with those of heparin, a clinically established anticoagulant, and the results are summarized in Table 2. The PT assay demonstrated a concentration-dependent prolongation of clotting time following AgNP treatment. PT values increased from approximately 14s in the untreated control to nearly 20s at 75 µg/mL AgNPs. In comparison, heparin exhibited a substantially stronger anticoagulant effect, extending PT values from approximately 95s at 25 µg/mL

Table 1 Quantitative Analysis of Wound Closure and Migration of Vero Cells Treated with Biosynthesized Silver Nanoparticles (AgNPs) During the in vitro Scratch Wound-Healing Assay

Cells	0 h		24 h		48 h		Wound Closure (% um^2)	Area Difference (%)
	Area	Width	Area	Width	Area	Width		
Control mean	789.33	788.39	698.33	697.44	281.16	280.18	64.37±15.30	50.81
AgNPs mean	771.66	770.73	735.83	734.93	505.16	504.46	34.53±12.25**	26.65

Notes: Data are presented as mean values. Wound closure (%) was calculated relative to the initial wound area at 0 h. **$P < 0.01$ versus control at 48 h.

https://doi.org/10.2147/IJN.S612998

Table 2 Effect of Biosynthesized Silver Nanoparticles (AgNPs) on Prothrombin Time (PT) and Activated Partial Thromboplastin Time (APTT) Compared with Heparin-Treated Plasma

	Concentration (ug/mL)	AgNPs	Control (Heparin)
PT (Sec)	0	12±1.47	12±1.55
	25	15.3±1.39 ^{ns}	94±0.82****
	50	16.5±1.77 ^{ns}	125±2.16****
	75	17.87±0.95 ^{ns}	141±2.04****
PTT (Sec)	0	26±2.05	26±1.47****
	25	30±1.143 ^{ns}	119±2.12****
	50	46±1.56****	132±1.77****
	75	51±0.82****	152±1.84****

Notes: Data are presented as mean ± SD (n = 3). Statistical analysis was performed using two-way ANOVA followed by Tukey's multiple comparisons test. Statistical significance was determined relative to the corresponding control group: ns, not significant ($P > 0.05$); ****$P < 0.0001$.
Abbreviations: PT, prothrombin time; APTT, activated partial thromboplastin time; AgNPs, silver nanoparticles.

to 142s at 75 µg/mL. Two-way ANOVA revealed highly significant effects of both concentration and treatment type on PT values, with a significant interaction between these factors. Concentration accounted for 24.52% of the total variation, whereas treatment type contributed 54.68%. Tukey's multiple comparisons test indicated no significant differences among the AgNP concentrations, whereas highly significant differences were observed among all heparin concentrations ($P < 0.0001$), reflecting the stronger concentration-dependent effect of heparin. A similar trend was observed in the APTT assay. The APTT values increased progressively from approximately 28s in the control group to nearly 52s at 75 µg/mL AgNPs. In contrast, heparin markedly prolonged clotting time, increasing APTT values from approximately 120s at 25 µg/mL to nearly 155s at 75 µg/mL. Statistical analysis showed highly significant effects of concentration and treatment type on APTT values, with a significant interaction between both factors. Concentration contributed 33.91% of the total variation, while treatment type accounted for 49.24%. Tukey's test demonstrated significant differences among most AgNP concentrations, except between the control and 25 µg/mL groups, whereas all heparin concentrations differed significantly from one another. Although the anticoagulant effect of the biosynthesized AgNPs was lower than that of heparin, the concentration-dependent prolongation of both PT and APTT indicates that the nanoparticles interfere with multiple stages of the coagulation cascade. The simultaneous extension of PT and APTT suggests that AgNPs may influence both the extrinsic and intrinsic coagulation pathways. Several mechanisms have been proposed to explain the anticoagulant activity of silver nanoparticles. AgNPs can adsorb plasma proteins onto their surface, forming a protein corona that alters the availability and activity of coagulation factors. In particular, interactions with fibrinogen, thrombin, and other clotting proteins may inhibit fibrin polymerization and delay clot formation. Previous studies have also shown that metallic nanoparticles can modulate platelet activation, interfere with coagulation factor activity, and alter endothelial cell responses through surface-mediated interactions with blood proteins.[26]

Additionally, silver nanoparticles have been reported to promote fibrinolytic processes through indirect activation of plasmin-generating pathways, facilitating the degradation of fibrin networks and contributing to prolonged clotting times.[70] The relatively small size of the synthesized AgNPs (7–55 nm) may further enhance these effects by increasing the available surface area for interaction with plasma proteins and coagulation factors. Furthermore, the biomolecular capping layer identified by FTIR analysis may contribute to the observed anticoagulant activity through additional interactions with blood components. The present findings are consistent with previous reports describing anticoagulant properties of biologically synthesized silver nanoparticles.[26,34] Abdelgadir et al,[51] reported that AgNPs synthesized using *Lactobacillus salivarius* exhibited promising anticoagulant and thrombolytic activities, supporting the growing evidence that probiotic-mediated AgNPs can modulate hemostatic processes Similar observations have been reported for other biologically synthesized metallic nanoparticles, highlighting their potential as blood-compatible nanomaterials and alternative antithrombotic agents. Overall, the biosynthesized AgNPs produced by *L. brevis* exhibited moderate but

significant anticoagulant activity, as evidenced by the concentration-dependent prolongation of PT and APTT values. Although their anticoagulant effect was weaker than that of heparin, the ability of these nanoparticles to modulate both intrinsic and extrinsic coagulation pathways, together with their demonstrated antioxidant, wound-healing, and anticancer activities, highlights their potential as multifunctional nanomaterials for future biomedical applications.

Conclusion

This study demonstrates the successful green synthesis of AgNPs using the probiotic bacterium *L. brevis* as a biological reducing and stabilizing agent, highlighting its potential as a sustainable microbial nanofactory for nanoparticle production. The biosynthesized AgNPs were successfully characterized by UV–Vis spectroscopy, FTIR, TEM, SAED, and zeta potential analysis. The nanoparticles exhibited a characteristic SPR peak at 410 nm, predominantly spherical morphology, crystalline structure, and particle sizes ranging from 7 to 55 nm with an average diameter of 27.18 ± 12.7 nm. Although the measured zeta potential (−2.57 mV) indicated weak electrostatic stabilization, FTIR analysis confirmed the presence of a biomolecular capping layer that likely contributed to colloidal stability through steric effects. Biological evaluation revealed that the synthesized AgNPs possess multifunctional activities. The nanoparticles exhibited strong concentration-dependent antioxidant activity, significant cytotoxic and antiproliferative effects against MCF-7 and HepG2 cancer cell lines, moderate wound-healing activity in the scratch assay, and measurable anticoagulant effects through prolongation of PT and APTT clotting times. These biological properties are likely associated with the combined influence of the nanoscale dimensions, crystalline silver core, and surface-associated biomolecules derived from *L. brevis* metabolites. Importantly, this work addresses a current knowledge gap regarding the use of *L. brevis* for the biosynthesis of multifunctional AgNPs and expands the growing body of evidence supporting probiotic-mediated nanotechnology as an environmentally friendly alternative to conventional nanoparticle synthesis methods. While the in vitro findings demonstrate promising biomedical potential, further studies are required to elucidate the underlying molecular mechanisms, optimize nanoparticle stability and dosage, evaluate selectivity toward normal and cancerous cells, and confirm safety and efficacy through in vivo investigations. Overall, the present study establishes *L. brevis*-derived AgNPs as promising multifunctional nanomaterials with potential applications in biomedical, pharmaceutical, and therapeutic fields.

Data Sharing Statement

Data will be given upon request.

Author Contributions

All authors made a significant contribution to the work reported, whether that is in the conception, study design, execution, acquisition of data, analysis and interpretation, or in all these areas; took part in drafting, revising or critically reviewing the article; gave final approval of the version to be published; have agreed on the journal to which the article has been submitted; and agree to be accountable for all aspects of the work.

Funding

This research received no external funding.

Disclosure

The authors declare that they have no known competing financial interests or personal relationships that could have appeared to influence the work reported in this paper.

References

1. Isah M. Recent advancement of nanomaterials: properties, fabrication, and applications. *Plant Biotechnol Persa*. 2025;7(3):148–163. doi:10.61186/pbp.7.3.148
2. Shibil S, Aparna C. *Metal Nanoparticles: Synthesis, Characteristics, and Applications*. Metal and Metal Oxide Nanoparticles CRC Press; 2026:1–16.

3. Devi L, Kushwaha P, Ansari TM, et al. Recent trends in biologically synthesized metal nanoparticles and their biomedical applications: a review. *Biol Trace Elem Res*. 2024;202(7):3383–3399. doi:10.1007/s12011-023-03920-9
4. Mendes C, Thirupathi A, Corrêa ME, et al. The use of metallic nanoparticles in wound healing: new perspectives. *Int J Mol Sci*. 2022;23 (23):15376. doi:10.3390/ijms232315376
5. Naseer Q, Xue X, Wang X, et al. Synthesis of silver nanoparticles using *Lactobacillus bulgaricus* and assessment of their antibacterial potential. *Braz J Biol*. 2022;82:e232434.
6. Lela AM, El-Sehrawy HM, Abdel-Rahman AM, et al. Efficiency evaluation and characterization of microbially, phyto and chemically synthesized silver nanoparticles. *Res J Pharm Technol*. 2024;17(2):717–722. doi:10.52711/0974-360X.2024.00111
7. Sati A, Mali SN, Ranade TN, et al. Silver nanoparticles (AgNPs) as a double-edged sword: synthesis, factors affecting, mechanisms of toxicity and anticancer potentials—An updated review till march 2025. *Biol Trace Elem Res*. 2026;204(1):401–452. doi:10.1007/s12011-025-04688-w
8. Tawo OE, Mbamalu MI. Advancing waste valorization techniques for sustainable industrial operations and improved environmental safety. *Int J Sci Res Arch*. 2025;14(2):127–149. doi:10.30574/ijsra.2025.14.2.0334
9. Soenen SJ, Parak WJ, Rejman J, et al. (Intra) cellular stability of inorganic nanoparticles: effects on cytotoxicity, particle functionality, and biomedical applications. *Chem Rev*. 2015;115(5):2109–2135. doi:10.1021/cr400714j
10. Madani M, Hosny S, Alshangiti DM, et al. Green synthesis of nanoparticles for varied applications: green renewable resources and energy-efficient synthetic routes. *Nanotechnol Rev*. 2022;11(1):731–759. doi:10.1515/ntrev-2022-0034
11. Kirubakaran D, Wahid JBA, Karmegam N, et al. A comprehensive review on the green synthesis of nanoparticles: advancements in biomedical and environmental applications. *Biomed Mater Devices*. 2026;4(1):388–413. doi:10.1007/s44174-025-00295-4
12. Vaseghi Z, Nematollahzadeh A, Tavakoli O. Green methods for the synthesis of metal nanoparticles using biogenic reducing agents: a review. *Rev Chem Eng*. 2018;34(4):529–559. doi:10.1515/revce-2017-0005
13. Hassan MG, El-Waseif AA, Abd El Gawad RH, et al. Assessment of antibacterial, cytotoxicity and wound healing influence of copper nanoparticles synthesized using probiotic bacteria. *Res J Pharm Technol*. 2023;16(10):4537–4542. doi:10.52711/0974-360X.2023.00739
14. Abatenh E, Gizaw B, Tsegay Z, et al. Health benefits of probiotics. *J Bacteriol Infec Dis*. 2018;2(1).
15. Abd-Elwahed ES, El-Waseif AA, Maany DA. Biosynthesis and FPLC purification of antibacterial peptide from the biotherapeutic agent. *Egypt Pharm J*. 2023;22(2):202–208. doi:10.4103/epj.epj_143_22
16. Maany D, Amr E-W, Abd El-Wahed E. Optimization of enterocin production from probiotic *Enterococcus faecium* using Taguchi experimental design. *Turk J Pharm Sci*. 2024;21(3):192. doi:10.4274/tjps.galenos.2023.83451
17. Dakhil AS. Biosynthesis of silver nanoparticle (AgNPs) using Lactobacillus and their effects on oxidative stress biomarkers in rats. *J King Saud Univ Sci*. 2017;29(4):462–467. doi:10.1016/j.jksus.2017.05.013
18. Veeraraghavan VP, Periadurai ND, Karunakaran T, et al. Green synthesis of silver nanoparticles from aqueous extract of Scutellaria barbata and coating on the cotton fabric for antimicrobial applications and wound healing activity in fibroblast cells (L929). *Saudi J Biol Sci*. 2021;28 (7):3633–3640. doi:10.1016/j.sjbs.2021.05.007
19. Tran HD, Moonshi SS, Xu ZP, et al. Influence of nanoparticles on the haemostatic balance: between thrombosis and haemorrhage. *Biomater Sci*. 2022;10(1):10–50. doi:10.1039/D1BM01351C
20. de Man J, Rogosa de M, Sharpe ME. A medium for the cultivation of *Lactobacilli*. *J Appl Microbiol*. 1960;23(1):130–135.
21. Hegazy A-WA, El-Waseif AA, Maany DA. Isolation, characterization, and molecular identification of probiotics showing promising hypoglycemia operating activities. *Egypt Pharm J*. 2023;22(1):105–110. doi:10.4103/epj.epj_137_22
22. Tamura K, Nei M. Estimation of the number of nucleotide substitutions in the control region of mitochondrial DNA in humans and chimpanzees. *Mol Biol Evol*. 1993;10(3):512–526. doi:10.1093/oxfordjournals.molbev.a040023
23. Saitou N, Nei M. The neighbor-joining method: a new method for reconstructing phylogenetic trees. *Mol Biol Evol*. 1987;4(4):406–425. doi:10.1093/oxfordjournals.molbev.a040454
24. Kumar S, Stecher G, Suleski M, et al. MEGA12: molecular evolutionary genetic analysis version 12 for adaptive and green computing. *Mol Biol Evol*. 2024;41(12):msae263. doi:10.1093/molbev/msae263
25. El-Waseif AA, Alshehrei F, Al-Ghamdi SB, et al. Antioxidant and anticoagulant activity of microbial nano cellulose-ZnO-Ag composite components. *Pak J Biol Sci PJBS*. 2022;25(6):531–536. doi:10.3923/pjbs.2022.531.536
26. Sharma V, Verma D, Okram GS. Influence of surfactant, particle size and dispersion medium on surface plasmon resonance of silver nanoparticles. *J Phys: Condens Matter*. 2020;32(14):145302. doi:10.1088/1361-648X/ab601a
27. Patel K, Bharatiya B, Mukherjee T, et al. Role of stabilizing agents in the formation of stable silver nanoparticles in aqueous solution: characterization and stability study. *J Dispers Sci Technol*. 2017;38(5):626–631. doi:10.1080/01932691.2016.1185374
28. EL-Ghwas DE. Characterization and biological synthesis of zinc oxide nanoparticles by new strain of Bacillus foraminis. *Biodiversitas J Biol Divers*. 2022;23(1).
29. Huang DJ, Hsien-Jung C, Chun-Der LI, et al. Antioxidant and antiproliferative activities of water spinach (*Ipomoea aquatica* Forsk) constituents. *Bot Bull Acad Sin*. 2005;46.
30. Lateef A, Ojo SA, Akinwale AS, et al. Biogenic synthesis of silver nanoparticles using cell-free extract of *Bacillus safensis* LAU 13: antimicrobial, free radical scavenging and larvicidal activities. *Biologia*. 2015;70(10):1295–1306. doi:10.1515/biolog-2015-0164
31. Senthilraja P, Kathiresan K. In vitro cytotoxicity MTT assay in Vero, HepG2 and MCF-7 cell lines study of Marine Yeast. *J Appl Pharm Sci*. 2015;5 (3):080–084. doi:10.7324/JAPS.2015.50313
32. El-Waseif AA, El-Ghwas DE. Anti-breast cancer and cytotoxicity of nano materials formed bacterial cellulose-ZnO-Ag composite. *Mater Today Proc*. 2022;60:1651–1655. doi:10.1016/j.matpr.2021.12.193
33. Liang -C-C, Park AY, Guan J-L. In vitro scratch assay: a convenient and inexpensive method for analysis of cell migration in vitro. *Nat Protoc*. 2007;2(2):329–333. doi:10.1038/nprot.2007.30
34. El-Waseif AA, Ahmed SZ, Waheeb HO, et al. Correlation of probiotic synthesis nanoparticles against rift valley fever vector, *Culex antennatus* becker (Diptera: culicidae). *Res J Pharm Technol*. 2023;16(6):2969–2974. doi:10.52711/0974-360X.2023.00490
35. Garmasheva I, Kovalenko N, Voychuk S, et al. Lactobacillus species mediated synthesis of silver nanoparticles and their antibacterial activity against opportunistic pathogens in vitro. *Bioimpacts*. 2016;6(4):219. doi:10.15171/bi.2016.29

36. Ahmad F, Ashraf N, Ashraf T, et al. Biological synthesis of metallic nanoparticles (MNPs) by plants and microbes: their cellular uptake, biocompatibility, and biomedical applications. *Appl Microbiol Biotechnol*. 2019;103(7):2913–2935. doi:10.1007/s00253-019-09675-5
37. Kalimuthu K, Babu RS, Venkataraman D, et al. Biosynthesis of silver nanocrystals by Bacillus licheniformis. *Colloids Surf B Biointerfaces*. 2008;65(1):150–153. doi:10.1016/j.colsurfb.2008.02.018
38. Maqsoodi M, Tajbakhsh E, Momtaz H. Green biosynthesis and antimicrobial activity of silver nanoparticles synthesized by *Lactobacillus acidophilus* against multidrug-resistant *Klebsiella pneumoniae*. *BMC Biotechnol*. 2025;25(1):133. doi:10.1186/s12896-025-01018-9
39. Kim S, Ryu D. Silver nanoparticle-induced oxidative stress, genotoxicity and apoptosis in cultured cells and animal tissues. *J Appl Toxicol*. 2013;33 (2):78–89. doi:10.1002/jat.2792
40. Syame SM, Mansour AS, Khalaf DD, et al. Green synthesis of silver nanoparticles using lactic acid bacteria: assessment of antimicrobial activity. *Worlds Vet J*. 2020;10(4):625–633. doi:10.54203/scil.2020.wvj75
41. Coronado EA, Encina ER, Stefani FD. Optical properties of metallic nanoparticles: manipulating light, heat and forces at the nanoscale. *Nanoscale*. 2011;3(10):4042–4059. doi:10.1039/c1nr10788g
42. Wang L, Hasanzadeh Kafshgari M, Meunier M. Optical properties and applications of plasmonic-metal nanoparticles. *Adv Funct Mater*. 2020;30 (51):2005400. doi:10.1002/adfm.202005400
43. Das D, Nath BC, Phukon P, et al. Synthesis of ZnO nanoparticles and evaluation of antioxidant and cytotoxic activity. *Colloids Surf B Biointerfaces*. 2013;111:556–560. doi:10.1016/j.colsurfb.2013.06.041
44. Valgimigli L, Baschieri A, Amorati R. Antioxidant activity of nanomaterials. *J Mater Chem B*. 2018;6(14):2036–2051. doi:10.1039/C8TB00107C
45. Indrianingsih AW, Rosyida VT, Apriyana W, et al. Antioxidant and antibacterial properties of bacterial cellulose—Indonesian plant extract composites for mask sheet. *J Appl Pharm Sci*. 2020;10(7):037–042.
46. Tyavambiza C, Meyer M, Wusu AD, et al. The antioxidant and in vitro wound healing activity of cotyledon orbiculata aqueous extract and the synthesized biogenic silver nanoparticles. *Int J Mol Sci*. 2022;23(24):16094. doi:10.3390/ijms232416094
47. Akter M, Sikder MT, Rahman MM, et al. A systematic review on silver nanoparticles-induced cytotoxicity: physicochemical properties and perspectives. *J Adv Res*. 2018;9:1–16. doi:10.1016/j.jare.2017.10.008
48. Zhang X-F, Liu Z-G, Shen W, et al. Silver nanoparticles: synthesis, characterization, properties, applications, and therapeutic approaches. *Int J Mol Sci*. 2016;17(9):1534. doi:10.3390/ijms17091534
49. Rai M, Yadav A, Gade A. Silver nanoparticles as a new generation of antimicrobials. *Biotechnol Adv*. 2009;27(1):76–83. doi:10.1016/j.biotechadv.2008.09.002
50. Mohammed AA, Hegazy A, Salah A. Novelty of synergistic and cytotoxicity activities of silver nanoparticles produced by *Lactobacillus acidophilus*. *Appl Nanosci*. 2023;13(1):633–640. doi:10.1007/s13204-021-01878-5
51. Abdelgadir A, Adnan M, Patel M, et al. Probiotic *Lactobacillus salivarius* mediated synthesis of silver nanoparticles (AgNPs-LS): a sustainable approach and multifaceted biomedical application. *Heliyon*. 2024;10(18):e37987. doi:10.1016/j.heliyon.2024.e37987
52. Devi J, Bhimba B. Anticancer Activity of Silver Nanoparticles Synthesized by the Seaweed Ulva lactuca Invitro. 1: 242. 242 Page 2 of 5 Volume 1• Issue 4• 2012 silver nitrate solution was added to the filtrate slowly under magnetic stirring conditions for even coating of silver and subjected to heating at 12 C for 10 min. Extr Used Reducing Stab Agent 1mM Silver Nitrate This One Pot Green Synth Was Modif Method Follow Vigneshwaran Al18. 2012.
53. Inbathamizh L, Ponnu TM, Mary EJ. In vitro evaluation of antioxidant and anticancer potential of *Morinda pubescens* synthesized silver nanoparticles. *J Pharm Res*. 2013;6(1):32–38.
54. Siddiqui AJ, Patel M, Jahan S, et al. Silver nanoparticles derived from probiotic *Lactobacillus casei*—A novel approach for combating bacterial infections and cancer. *Probiotics Antimicrob Proteins*. 2025;17(3):1277–1294. doi:10.1007/s12602-023-10201-3
55. Ravi AK, Muthukrishnan S, Gunasangkaran G, et al. Biosynthesis of chitosan encapsulated silver-nanoparticles using Probiotic-*Lactobacillus plantarum* strain and it's in vitro anticancer assessment on HeLa cells. *Med Microecol*. 2024;22:100117. doi:10.1016/j.medmic.2024.100117
56. Yuksekdag Z, Kilickaya R, Kara F, et al. Biogenic-Synthesized silver nanoparticles using the *Ligilactobacillus salivarius* KC27L postbiotic: antimicrobial, Anti-Biofilm, and antioxidant activity and cytotoxic effects. *Probiotics Antimicrob Proteins*. 2025;17(5):3685–3699. doi:10.1007/s12602-025-10481-x
57. Pasha A, Kumbhakar DV, Sana SS, et al. Role of biosynthesized Ag-NPs using *Aspergillus niger* (MK503444. 1) in antimicrobial, anti-cancer and anti-angiogenic activities. *Front Pharmacol*. 2022;12:812474. doi:10.3389/fphar.2021.812474
58. Jadhav K, Deore S, Dhamecha D, et al. Phytosynthesis of silver nanoparticles: characterization, biocompatibility studies, and anticancer activity. *ACS Biomater Sci Eng*. 2018;4(3):892–899. doi:10.1021/acsbiomaterials.7b00707
59. Ali SA, Osman ME, Mohamed ET. Eco-friendly biosynthesis of silver nanoparticles using marine-derived fusarium exquisite: optimization, characterization, and evaluation of antimicrobial, antioxidant, and cytotoxic activities. *World J Microbiol Biotechnol*. 2025;41(5):165. doi:10.1007/s11274-025-04368-w
60. Al-Janabi ZMJ, Al-dulaimy WYM, Hekmat M, et al. Examining the cytotoxic effects of a biosurfactant from *Lactobacillus plantarum* and biosynthesised silver nanoparticles on a breast cancer cell line. n.d.
61. Nguyen LAT, Van Mai B, Van Nguyen D, et al. Green synthesis of silver nanoparticles using *Callisia fragrans* leaf extract and its anticancer activity against MCF-7, HepG2, KB, LU-1, and MKN-7 cell lines. *Green Process Synth*. 2023;12(1):20230024. doi:10.1515/gps-2023-0024
62. Al Baloushi KSY, Senthilkumar A, Kandhan K, et al. Green synthesis and characterization of silver nanoparticles using *Moringa peregrina* and their toxicity on MCF-7 and Caco-2 human cancer cells. *Int J Nanomed*;2024. 3891–3905. 10.2147/IJN.S451694
63. Ullah I, Khalil AT, Zia A, et al. Insight into the molecular mechanism, cytotoxic, and anticancer activities of phyto-reduced silver nanoparticles in MCF-7 breast cancer cell lines. *Microsc Res Tech*. 2024;87(7):1627–1639. doi:10.1002/jemt.24540
64. Chahardoli A, Karimi N, Fattahi A. Biosynthesis, characterization, antimicrobial and cytotoxic effects of silver nanoparticles using Nigella arvensis seed extract. *Iran J Pharm Res IJPR*. 2017;16(3):1167.
65. Abdel-Rahman LH, Al-Farhan BS, Abou El-ezz D, et al. Green biogenic synthesis of silver nanoparticles using aqueous extract of moringa oleifera: access to a powerful antimicrobial, anticancer, pesticidal and catalytic agents. *J Inorg Organomet Polym Mater*. 2022;32(4):1422–1435. doi:10.1007/s10904-021-02186-9
66. Ahsan A, Farooq MA, Ahsan Bajwa A, et al. Green synthesis of silver nanoparticles using Parthenium hysterophorus: optimization, characterization and in vitro therapeutic evaluation. *Molecules*. 2020;25(15):3324. doi:10.3390/molecules25153324

67. Sivakumar M, Surendar S, Jayakumar M, et al. *Parthenium hysterophorus* mediated synthesis of silver nanoparticles and its evaluation of antibacterial and antineoplastic activity to combat liver cancer cells. *J Clust Sci*. 2021;32(1):167–177. doi:10.1007/s10876-020-01775-x
68. Castro Aceituno V, Ahn S, Simu SY, et al. Silver nanoparticles from *Dendropanax morbifera* Léveille inhibit cell migration, induce apoptosis, and increase generation of reactive oxygen species in A549 lung cancer cells. *Vitro Cell Dev Biol-Anim*. 2016;52(10):1012–1019. doi:10.1007/s11626-016-0057-6
69. Vijayakumar G, Kim HJ, Rangarajulu SK. In vitro antibacterial and wound healing activities evoked by silver nanoparticles synthesized through probiotic bacteria. *Antibiotics*. 2023;12(1):141. doi:10.3390/antibiotics12010141
70. Cheng R, Huang W, Huang L, et al. Acceleration of tissue plasminogen activator-mediated thrombolysis by magnetically powered nanomotors. *ACS Nano*. 2014;8(8):7746–7754. doi:10.1021/nn5029955